Preparation and Characterization of CdZnTe Coplanar Grid Detectors

---

Fabrication and Characterization
of CZT Coplanargrid detector
Doctor of Philosophy
by
Giacomo Benassi

Universita' di Parma
2010

wò qù dàxué

Table of Contents

Chapter 1: Introduction **1**

Chapter 2: Radiation Sources and Radiation Interactions **3**

2.1 Radiation . . . 3

2.2 Radiation Source . . . 4

2.2.1 Alpha particles . . . 4

2.2.2 Gamma Radiation . . . 4

2.3 Interactions with matter . . . 5

2.3.1 Alpha Particles Interaction . . . 5

2.3.2 Gamma Ray Interaction . . . 5

2.3.2.1 Exponential Attenuation . . . 6

2.3.2.2 Photoelectric Effect . . . 6

2.3.2.3 Compton Scattering . . . 7

2.3.2.4 Pair Production . . . 7

Chapter 3: Semiconductor detectors for gamma-ray spectroscopy **8**

3.1 General Feature of Radiation Detectors . . . 8

3.1.1 Detector for Gamma-rays . . . 9

3.2 Semiconductor detectors . . . 10

3.3 Response Function . . . 11

3.3.1 Pulse Spectra . . . 11

3.3.2 Gamma interaction response . . . 12

3.3.3 Response in a real Detector . . . 13

3.4 Resolution of a Detector . . . 16

3.4.1 Energy resolution . . . 16

3.4.2 Spatial Resolution . . . 18

Chapter 4: CdZnTe **19**

4.1 CZT as Gamma detector . . . 19

4.1.1 II-VI semiconductors . . . 19
4.1.1.1 $Cd_{(1-x)}Zn_xTe$ . . . 20
4.1.2 Transport Property . . . 21
4.2 Growth . . . 22

Chapter 5: The Signal **23**
5.1 Signal Formation . . . 23
5.1.1 The effect of trapping in the charge collection . . . 25
5.1.2 Ramo-Shockley Theorem . . . 26
5.1.3 Planar geometry . . . 27
5.1.4 Coplanar-Grid . . . 28
5.1.4.1 Resolution . . . 32
5.2 The Signal Acquisition . . . 32
5.3 Signal Processing . . . 36

Chapter 6: Experimental Setup **38**
6.1 Detector . . . 38
6.1.1 Detector Preparation . . . 38
6.1.1.1 Surface Preparation . . . 39
6.1.1.2 Contact Preparation . . . 39
6.1.1.3 Passivation Process . . . 40
6.1.1.4 Pcboard and metal box . . . 41
6.2 Preamplifier . . . 41
6.3 Amplifier . . . 42
6.4 Multichannel analyzers (MCA) . . . 42
6.5 Calibration Procedure . . . 42

Chapter 7: Experimental Result **45**
7.1 IV characteristic . . . 45
7.2 Transport Properties . . . 46
7.3 Measure of $\mu\tau$ . . . 47
7.4 Time Of Flight (TOF) . . . 50
7.5 Spectroscopic Performance . . . 53
7.5.1 Spectroscopic measure . . . 53
7.5.1.1 Correcting system for high resolution spectra. . . . 56

7.5.1.2 ^{241}Am S068.PH 59
7.5.1.3 ^{57}Co S306.PH 61
7.5.1.4 Gain Correction 61
7.5.1.5 ^{137}Cs S227.PH 62
7.5.2 Nature of the high energy tail 65
7.5.3 List of the sources 67

Chapter 8: Conclusion **69**

References **75**

Chapter I

Introduction

Il presente lavoro di tesi è frutto di una collaborazione tra l'istituto IMEM CNR di Parma ed il dipartimento di Radiation Physics presso l'Università del Surrey in Inghilterra. Il lavoro rientra in un progetto più ampio che comprende appunto lo sviluppo e il miglioramento di detector basati sul CdZnTe (CZT). In particolare i campioni di CZT sono stati cresciuti nell'istituto IMEM di Parma tramite la tecnica Boron oxide full encapsulate veritcal Bridgman, mentre tutta la parte che concerne il detector processing e la sua caratterizzazione sono state effettuate nella Surrey University. Il lavoro di tesi è il frutto di questa seconda parte di frabbricazione e caratterizazzione dei dispositivi.
L'interesse del CZT (semiconduttore II-VI) è infatti giustificata dalle interessanti caratteristiche che lo rendono un ottimo candidato per lo sviluppo di detector per fotoni ad media ed alta energia (). Le sue principali caratteristiche sono: alto numero atomico, alta resistività, alto stopping power e un valore di band gap abbastanza elevato da consentire il suo utilizzo a temperatura ambiente (al contrario di Si e Ge). Nonostante l'alta resistività il CZT però mostra buone proprietà di trasporto soprattutto elettroniche. Per quanto riguarda quelle lacunari invece, la tecnologia di crescita non è ancora in grado di fornire cristalli con elevate proprietà di trasporto lacunare che, quindi, rimangono almeno un ordine di grandezza inferione a quelle elettroniche. Queste basse proprietà di trasporto possono influenzare notevolmente la risposta del detector limitandone in particolare la sua risoluzione. In questo contesto sono quindi nate delle tecniche in grado di eliminare il contributo lacunare nella risposta complessiva del detector: si parla di single polarity sensing detectors. Una di queste tecniche è appunto la Coplanar-Grid proposta da Luke nel 1994. Il suo principio di fuzionamento è identico alla griglia di Frish utilizzata nei detector a gas ma, nel caso dei dispositivi a semiconduttore, invece di inserire una griglia metallica all'interno del cristallo, si utilizza la sottrazione di due segnali provenienti da due griglie indipendenti (ed interdigitate) che formano l'anodo del dispositivo. Le griglie sono mantenute ad una differenza di potenziale tra loro mentre il catodo è rappresentato da un contatto planare. Grazie a questa

configurazione degli elettrodi è quindi possibile eliminare il contributo lacunare dal segale e lasciando perciò solo quello elettronico (singola polarità).
La prima del lavoro è stata quella di fabbricazione di due Coplanar Grid detector. La realizzazione dei dispositivi è iniziata con la preparazione delle superfici tramite lappaggio meccanico e attacchi chimici. Poi tramite un processo di lift-off sono stati depositati i contatti coplanar grid e planari in platino (tramite un processo di sputtering). Infine i detector sono stati montati su pc board disegnate apposta dall'Università del Surrey e contattati grazie ad un wire bounder; infine il tutto è stato inserito in un box metallico adibito alle misure.La seconda parte invece è stata la caratterizzazione dei dispositivi che può essere riassunta anch'essa in due parti principali. Inizialmente sono state misurate le proprietà del bulk e superficiali dei campioni: in particolare caratteristiche IV dei contatti, resistenze di bulk e superficiali, proprietà di trasporto quali prodotto mobilità-tempo di vita e mobilità. Queste ultime sono state ricavate dalla risposta dei detector alle particelle alpha (^{241}Am).
La seconda parte del lavoro ha riguardato invece le misure spettroscopiche di diverse sorgenti gamma a diverse energie: nello specifico sono state utilizzate ^{241}Am, ^{57}Co e ^{137}Cs aventi rispettivamente emissioni gamma principali ad energie 59 KeV, 122 KeV e 662 KeV. Durante questa parte di misure si è cercato di migliorare le prestazioni del dispositivo in termini spettroscopici e soprattutto si sono analizzati i limiti dovuti alla tecnica coplanar-grid. In particolare è stato messo a punto un sistema di misura che correggesse la scarsa risoluzione dovuta alla non ottimizzata geometria dei contatti. La geometria infatti non è stato un parametro che si potesse ottimizare in quanto è stata disponibile un solo tipo di geometria Alla fine è stato possibile correlare le caratteristiche dei cristalli con le risposte dei detector, comparare i due dispositivi e proporre nuove caratteristiche per migliorare il funzionamento complessivo del detector. In accordo con la letteratura, è stata anche proposta una nuova geometria della Coplanar-Grid in modo da eliminare i problemi riscontrati in questo lavoro.

Chapter II

Radiation Sources and Radiation Interactions

2.1 Radiation

In this chapter is an introduction to radiation and its interactions with matter. Alpha sources were used to extract the transport properties of the bulk material and therefore were used to measure mobility-lifetime product ($\mu\tau$) and the time of flight (TOF) (chapter 7.3 and 7.4). The gamma sources were used for testing the detector performance (chapter 7.5).
Before starting with the explanation of the different type of radiation is better to introduce their relative units.

Activity

The activity A of a radioisotope source is defined as the rate of decays. This quantity depends linear on the number of radioactive nuclei N:

$$A = \frac{dN}{dt} = -\lambda N \tag{2.1}$$

where the constant λ is called decay constant. The SI unit of activity is the Becquerel (Bq) that means 1 disintegration per second.
In stead of calculating every time the activity of a source it is very useful the relation:

$$N = \frac{N_0}{2^{\frac{t}{t_{1/2}}}} \tag{2.2}$$

where N and N_0 are the activity at time $t_0 + t$ and at t_0. t is the time difference and $t_{1/2}$ is the half time.

Radioactive Half-Life

The radioactive half-life, for a given radioisotope, is the time after which half of the initial number of radioactive nuclei in the sample have undergone a radioactive decay. Therefore after 2 half lives, there will be 1/4 of the original radioactive material.

2.2 Radiation Source

In general there are several ways for an unstable nucleus to reach the ground state. The possible ways are: creation of charged particles like β and α, uncharged particles like neutrons or in form of electromagnetic radiation like γ-rays and X-rays.

2.2.1 Alpha particles

The alpha particles are a charged heavy particles. They are emitted from nuclei due to nuclear instability. Alpha particles constitute 2 protons and two neutrons like the nucleus of ^4He. The decay is schematically written as:

$$ {}^{A}_{Z}X \rightarrow {}^{A-4}_{Z-2}Y + {}^{4}_{2}\alpha \tag{2.3} $$

where X and Y are the initial and final nuclear species. Every decay is governed by a probability and a list of all the possible decays is available in all the nuclear physic books. The important feature α particle decay is the mono energetic emission. Typical alpha sources emit mono energetic radiation with energies in the range between $4MeV$ and $6MeV$. The problem is that the energy is strongly correlated to the half-life and precisely higher energy means lower half-time. On the other side lower energy means lower penetration inside matter and, for this reason, in the laboratories is common used sources around the value of $5MeV$.

2.2.2 Gamma Radiation

For seeking the lower energy level the excited nuclei can emit gamma rays. It is very common that the excited nuclei are created in a decay from a parent radionuclide. In fig the decay scheme of two sources with relative emission probability ("branching ratios")are shown. .The common case is a beta decay that provides the exited state. Therefore the gamma-rays have a half-time characteristic of the parent beta decay that normally is very long.

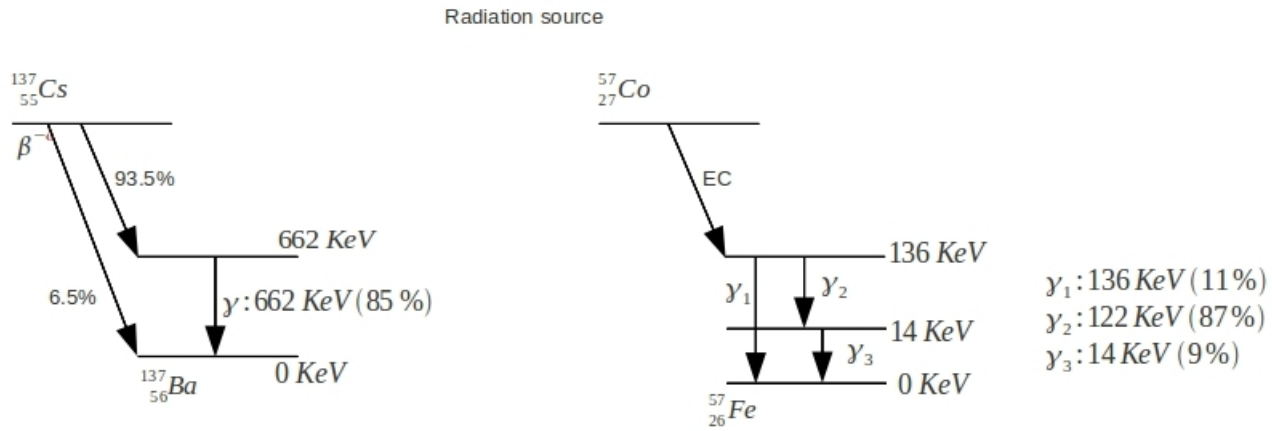

Figure 2.1: Two decay schemes for $^{137}_{55}Cs$ and $^{57}_{27}Co$,EC means electron capture. The value of gamma energy and their probability are taken by [Knoll]

2.3 Interactions with matter

2.3.1 Alpha Particles Interaction

Alpha particles are heavy positive charged particles and therefore can interact with every charge inside the material via coulomb interactions, in particular with bound electrons. In this case two possible processes, depending on the energy of the alpha particles, can take place. The first is excitation: the energy transferred raises the electron into a higher shell. The second is the ionization process: the electron is completely removed from the atom. This second can happen only if the energy is high enough. The maximum energy transferred depends on the ratio between the mass of the incident alpha particle and the electron mass. This value is very small and this fact suggests that the alphas can interact with a lot of electrons continuously decreasing their velocity. Linear stopping power S is defined as the rate of loss energy per unit path length:

$$S = -\frac{dE_\alpha}{dx} \tag{2.4}$$

2.3.2 Gamma Ray Interaction

Photons have zero rest mass and they are also a neutral, for this reason it is impossible to lose energy with Coulomb interactions. The interaction with the matter is therefore less with consequently more penetration into the material. The gamma radiation can travel a

considerable distance inside the matter: this penetration is governed by statistical factors that depend on the energy of the radiation and the nature of the material.

2.3.2.1 Exponential Attenuation

If mono energetic gamma radiation of intensity I_0 passes through an absorbing material of thickness l , than:

$$I = I_0 exp^{-\mu \cdot l} \tag{2.5}$$

where I is the intensity of the transmitted beam and μ is the linear attenuation coefficient. Formula (2.5) is called law of gamma ray attenuation. The attenuation coefficient depends on the gamma-ray energy, the atomic number and density of the absorber medium. In particular, as will be shown later, there are three dominant interactions phenomena, every one with a specific statistical probability. Another important quantity is the mean free path λ that represents the average distance traveled inside the medium and is given by:

$$\lambda = \frac{\int_0^\infty x exp^{-\mu x} dx}{\int_0^\infty exp^{-\mu x} dx} = \frac{1}{\mu} \tag{2.6}$$

The Three photon interactions are: photoelectric effect, Compton scattering and pair production. The relative probabilities are respectively τ,σ ,κ and the linear attenuation μ is the combination of all process:

$$\mu = \tau + \sigma + \kappa \tag{2.7}$$

2.3.2.2 Photoelectric Effect

In this interaction the energy of the incident photon is totally absorbed by atoms and the photon disappears. After the absorption the atom ejects an electron from one shell (usually K shell). The kinetic energy of the electron ejected is:

$$E_e = h\nu - E_b \tag{2.8}$$

where E_b is the binding energy and obviously depends on the type of shell. This process creates an ionized atom with a vacancy. This vacancy is quickly filled through the capture of a free electron or by rearranging the electronic shell in the atom. For this reason there may also be characteristic X-ray generation or other competitive processes like Auger emission. The photoelectric process is the dominant mode of interaction for gamma rays at low energy.

The probability is enhanced in general with the atomic number Z and is approximately equal to:

$$\tau \sim A \cdot \frac{Z^n}{E_\gamma^{3.5}} \tag{2.9}$$

Where A is a constant and the exponent n varies between 4 and 5.

2.3.2.3 Compton Scattering

This interaction involves an electron of the absorbed material. An incident gamma ray photon is deflected through an angle θ whit respect to its original direction. The photon hits the electron which is called recoil electron. In this case the photon does not disappear. The transferred energy depends on the interaction angle and so it can vary from zero to a large fraction of the gamma-ray energy.

$$E_e = E_\gamma - E' \tag{2.10}$$

where E_e is the kinetic energy of the scattered electron, E_γ the value of the energy of the incident photon and E' is the energy of the scattered γ-ray.

$$E' = \frac{E_\gamma}{1 + \frac{E_\gamma}{m_0 c^2}(1 - cos\theta)} \tag{2.11}$$

θ is the scattering angle and m_0c^2 (0.511 MeV) the rest-mass energy of the electron.
The Compton Scattering probability depends on the number of electrons available as scattering target and, therefore, increases linear with the atomic number $\sigma \propto Z$.

2.3.2.4 Pair Production

If the gamma photon, with a sufficiently large energy, passes near a nucleus it can disappear and its energy reappear as a positron and electron pair. The energy to create this pair is constant (1.02 MeV): only if the energy of the photon exceeds this value is this process available. There is no excitation of the nucleus during this interaction, the pair is created directly as energy/mass conversion. If the energy excess 1.02 MeV then this exceeds appears as kinetic energy.

$$E_{e^+} = E_{e^-} = \frac{E_\gamma - 1.022\,MeV}{2} \tag{2.12}$$

The probability κ magnitude varies approximately as $\approx Z^2$.

Chapter III

Semiconductor detectors for gamma-ray spectroscopy

3.1 General Feature of Radiation Detectors

Most radiation detectors can be approximated as a ionization chamber: the presence of radiation creates charged particles in the detection volume that are separated and collected by anode and cathode respectively biased. The ionization can be initiated by charged (α and β particles) or uncharged particles (for example X-rays and γ-rays). In this last case this ionization is due to an electron to which the radiation has transferred energy by one of the possible mechanisms discussed in chapter 2. In any case the ionizable medium can be made with different types of material: gases, liquids and solids. In table 3.1 are summarized some properties that characterize these different media. In general the desirable properties in a

	Gas	Liquid	Solid
Atomic number Z	low	moderate	moderate
Ionization energy ϵ_i	moderate	moderate	low
Density	low	moderate	high
Signal speed	moderate	moderate	fast

Table 3.1: Properties of different medium

detector are:

High density:

- high stopping power that means a decrease in the detection volume

Low ionization energy ϵ_i:

- increases the charge yield $\frac{dq}{dE}$

- increases the resolution $\frac{\Delta E}{E} \propto \sqrt{\epsilon_i}$ ((3.3.2)

High field in the detection volume

- improved charge collection efficiency (5.1.5)
- fast response(4.1.3.1)

As shown in table 3.1 the solid state and in particular semiconductors can have good qualities as detectors compared with other media. Another important feature, in addition to energy measurements, allowed by semiconductor detectors is the precision position sensing (2D or 3D). The resolution is, in fact, mainly determined by the precision in the lithography process and, therefore, it is in the order of tens μm.

3.1.1 Detector for Gamma-rays

The possible gamma interactions with matter are in general three (see chapter 2). Because x-ray and gamma-rays are invisible to the detector only the electrons created in the interaction provide the creation of a signal. Therefore, in order to measure the energy of incident radiation, it is very important that all the energy is deposited inside the detection volume. In this way the amplitude of the signal is directly connected to the energy of the incident radiation. Ideally if the detector volume is enough to absorb every secondary product of the interaction (like Compton scattered gamma ray, annihilation photons or characteristic X-rays) it would be indifferent in which manner the photon interacts because in all the case all the energy is deposited in the detector. But in the case of a real detector (finite dimensions) this condition is not always respected and, therefore, it is required to maximize the photoelectric effect events. In this interaction all the energy is transferred to one electron as kinetic energy. This fast particle can interact with the medium and transfer its energy by excitation and ionization of atoms and Bremsstrahlung emission. Also in this case the detector must be larger than the free path of this secondary electron but this is usually the case due to the short range of the electron. In addiction to the previously mentioned, a good X-ray and gamma-ray detector must carry out two roles:

- It must have a reasonable probability of interacting with incident rays with a good efficiency and ideally by Photoelectric effect .

- It must be a good detector for secondary electrons.

The probability of interaction depends directly by the energy of radiation but, for a fixed energy, it depends by the atomic number Z of detection material : in particular $\tau \propto Z^5$, $\sigma \propto Z$ and $\kappa \propto Z^2$. This means that materials with higher Z has more probability of Photoelectric interaction.

3.2 Semiconductor detectors

It is clear that some semiconductors are good candidates as radiation detector. The ionization energy in a semiconductor is smaller compared to other media. For this reason every secondary electron can excite a large number N of electrons creating electron-hole pairs (ehps) (10^4) in direct proportion to the energy deposited:

$$N \propto \frac{E_0}{\epsilon_i} \tag{3.1}$$

where E_0 is the energy deposited. The ionization energy depends directly on the value of the band gap energy E_g[C.A. Klein, J. Applied Physics 39 (1968) 2029]:low energy band gap means an increasing in the number of ehps created.
The detection volume must have a high field region to decrease the response time (velocity of the carriers) and increase the charge collection. The inconvenience due to high field is the leakage current (dark current) I_d due to the free charge inside the material. These carriers are generated by thermal excitation and therefore this process depends directly on the value of the energy gap. High value means low noise (low number of free carriers) and the possibility of working at room temperature unlike small band gap materials that need a cooling system to reduce the value of the dark current (Ge 0.67 eV). Thus high resistivity materials allow to have high field and low dark current at room temperature. In these materials the value of E_g is a compromise between few thermally generated carriers and high ionization energy. The main problem in these materials is to have high resistivity with good transport properties. For increasing the resistivity the crystals are grown with some impurities that can reduce the transport properties.
In figure 3.1 there is a comparison between the physical properties for different semiconductor materials used for detection:

Parameter	Si	GaAs	Ge	$Cd_{0.9}Zn_{0.1}Te$	CdTe
Density ($g\,cm^{-3}$)	2.33	5.32	5.33	5.78	5.85
Average atomic number(s)	14	31.5	32	49.1	50
Band gap (eV)	1.12	1.43	0.67	1.572	1.44
Pair creation energy (eV)	3.62	4.2	2.96	4.64	4.43
Electron mobility ($cm^2\,V^{-1}\,s$)	1400	8000	3900	1000	1100
Hole mobility ($cm^2\,V^{-1}\,s$)	1900	400	1900	120	100
Electron lifetime (s)	$>10^{-3}$	10^{-8}	$>10^{-3}$	3×10^{-6}	3×10^{-6}
Hole lifetime (s)	10^{-3}	10^{-7}	2×10^{-3}	1×10^{-6}	2×10^{-6}
Electron $\mu\tau$ product ($cm^2\,V^{-1}$)	>1	8×10^{-5}	>1	4×10^{-3}	3×10^{-3}
Hole $\mu\tau$ product ($cm^2\,V^{-1}$)	~1	4×10^{-6}	>1	1.2×10^{-4}	2×10^{-4}
Crystal structure	Cubic	Cubic (ZB)	Cubic	Cubic (ZB)	Cubic (ZB)
Lattice constant (Å)	5.4309	5.6533	5.64613		
Knoop hardness ($kg\,mm^{-2}$)	1150	750	692	?	60
Melting point (°C)	1412	1238	958	1092–1295	1092
Dielectric constant	11.7	12.8	16	10	10.9
Resistivity (Ω/cm)	$<10^4$	10^7	50	3×10^{10}	10^9
$1/e$ abs. Depth (mm) at 10 keV	0.127	0.051	0.050	0.011	0.011
at 100 keV	23.30	3.46	3.51	1.01	1.01
Typ. FWHM ΔE (keV) at 60 keV	0.4	0.7	0.3	1.5	1.1
Intrinsic. FWHM ΔE (keV) at 60 keV (Fano noise)	0.415	0.439	0.250	0.393	0.300
Typical thickness (mm)	0.3	0.2	20	2	2

Figure 3.1: Comparison for different semiconductors [A. Owens, A. Peacock / Nuclear Instruments and Methods in Physics Research A 531 (2004) 18–37]. In particular Si and Ge work only at low temperature due their to low band gap.

3.3 Response Function

3.3.1 Pulse Spectra

For radiation detection and, in particular, for spectroscopy measurements the detector works in a mode called "pulse mode" . In this type of operation it records every single event of interaction: this pulse of charge contains all the information about the single interaction event. The common way for displaying all the pulse is with a differential pulse height distribution. The abscissa is the linear pulse height and the ordinate is the differential number of pulse dN in a amplitude interval of dH. A typical spectrum is shown in fig 3.2. The integration over all the area will return the total number of pulses recorded:

$$N_0 = \int_0^\infty \frac{dN}{dH} dH \tag{3.2}$$

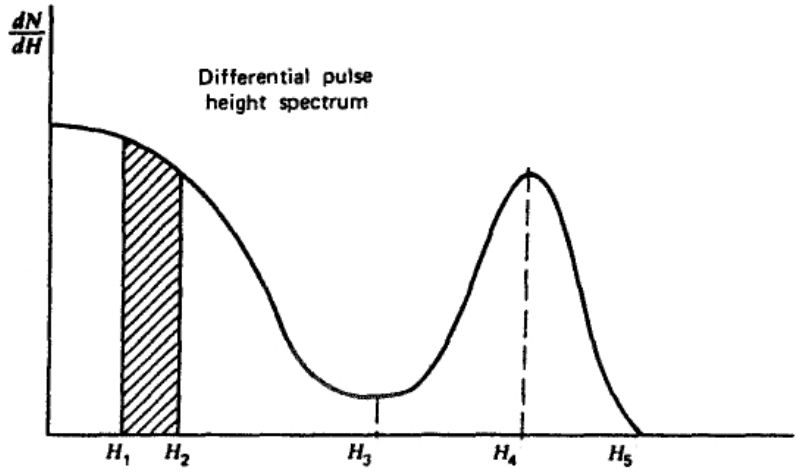

Figure 3.2: Differential Pulse Height Spectrum[3]

There is also an integral pulse height distribution but with differential distributions it is easier to discriminate subtle differences. For this reason it is more common to display the differential distribution.

3.3.2 Gamma interaction response

It is useful to analyze the pulse spectra concerning every interaction seen in chapter 2 in the case of a "small detector". In this case the detector is not large enough to absorb all the secondary scattered photons by Compton interaction.

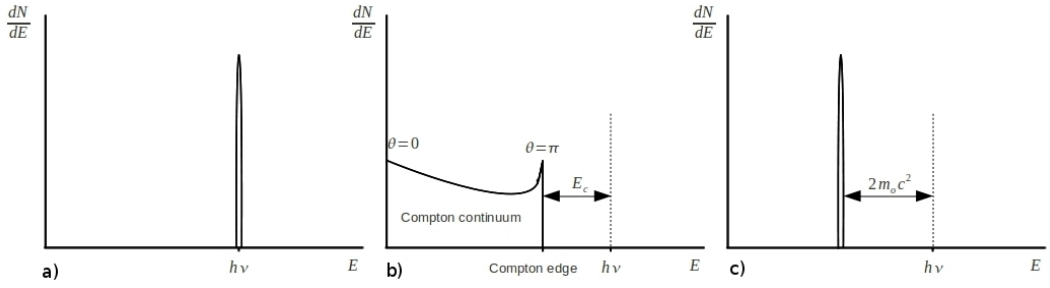

Figure 3.3: a)Photoelectric effect b)Compton effect c)Pair production

a) In the photoelectric effect the gamma photon disappears and a photoelectron is created (secondary electron). Normally this electron emerges from the K-shell. Due to conservation of the momentum the atom recoils in the process but this energy is too small and therefore neglected. Rearrangement of the ionized atom means emission of X-ray or Auger electron (more common in the first). Normally also in the "small detector" all the secondary radiation can be absorbed. The spectrum is simply a delta centered at the value of the gamma photon energy.

b) The result of a Compton interaction is a recoil electron and a scattered gamma-ray. The energy transferred depends on the scattering angle (2.11). The two extreme cases are 0 and π: in the first, a very small amount of energy is transferred to the electron ($\simeq 0$). The second case represents the maximum value of energy that can be transferred by the photon. In general all scattering angles are available and therefore the spectrum is a continuum distribution. In this case it is assumed that the photon after the interaction escape out of the detector without any other interaction.

c) In the pair production process the photon disappears due to the creation of an electron-positron pair, a minimum gamma ray energy is required to make the process possible (1.02 MeV). If the photon energy exceeds this value the excess energy is shared by the pair as kinetic energy. If the energy of the electron and positron is absorbed by the material (this is reasonable because they are charged particles) the response is a delta centered at a distance $2m_0c^2$ from the energy of incident photon.

In general in a material all this process act simultaneously and therefore the most common spectra is the sum of all this effect.

3.3.3 Response in a real Detector

in the real case the situation is more complicate. The main reason is that there are more type of interaction. In the follow discussion it is possible to exclude the pair product because the energies used in this project are than 1.02 MeV. Another important thing is also consider the surrounding materials because they can influence the response function of the detector. Normally in the way to reduce the natural background most gamma ray detector work inside a shielded box (for example Aluminum boxes). All these materials are a measurable sources of secondary radiation. Consequently the response of the detector depends by the type of

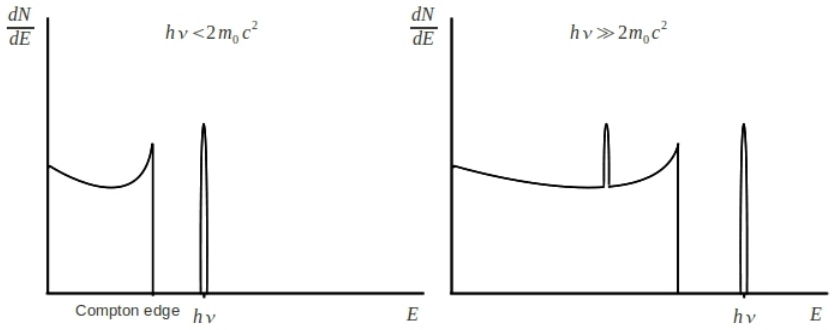

Figure 3.4: Pulse response with all the possible gamma-ray interactions

interaction that happens. All the possible interaction and their influence in the response spectra are showed in fig 3.5

1) The first peak 1 that appears in the spectra is due by surrounding material. If the photon doesn't interact with the detector it can interact with other material (metal box) in the same ways discussed in chapter 2. In the case of photoelectric interaction it is possible that a characteristic X-ray of the material can be detected by the detector. One characteristic peak (in general there is only one type of surrounding material) can appear at low energy in the response function.

2) The nature of peak 2 is similar as the case 1 but now the interaction is a Compton scattering. In this case is the scattered gamma-ray the particle detected by the detector. In the cases 1 and 2 the source of radiation is the surrounding material.

3) This process is the same discussed in the section before: scattering Compton figure b)

4) In the real case new events can be appear in the gap between the Compton edge and the photopeak: these events are due by multiple Compton interaction. In this types of event the Compton scattered photon can interact again with the detector: in particular in this case via another Compton interaction.

5) After the emission of a photoelectron the atom research the equilibrium by the emission of a characteristic X-ray (or Auger electron). If the photon absorption happens near the surface this secondary radiation can escape from the detector. Therefore these events

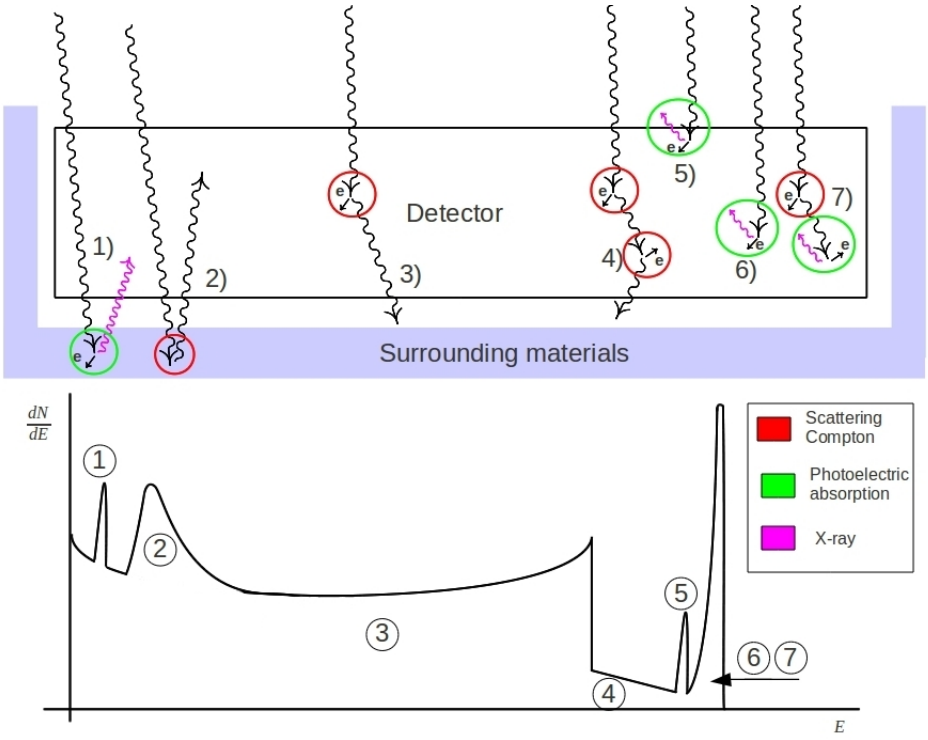

Figure 3.5: All the possible source of signal due by gamma-rays

appear with less energy than the photopeak: this gap is equal to the escaped X-ray (or Auger).

6) This is a photoelectric interaction as shown in figure a). These events form the photopeak that appear at the same energy (if the charge trapping is negligible) at the incident photons

7) Also in this type of interaction all the energy of the photons is deposited in the volume of the detector but in this case there are two interaction. The first is Compton scattering and the second is a photoelectric absorption of scattered Compton photon. Due to the high velocity of the light these two events appear like one in the electric signal.

3.4 Resolution of a Detector

3.4.1 Energy resolution

The energy resolution of a detector is the ability to resolve fine detail of the incident radiation. The easiest way to understand this important proprieties is examined its response to a mono energetic source of radiation. The response of detector in this case will be a distribution centered around an average pulse height H_0 (as 3.3 a)). For valuing the resolution is necessary to calculate the full width half maximum (FWHM) that represents the width of the distribution at a level that is just the half of the maximum peak (it's assumed that an eventual background it's just removed from the peak). The formal definition of energy resolution R is the ratio between FWHM and the value of the position of the peak H_0.

$$R = \frac{FWHM}{H_0} \tag{3.3}$$

The shape of the response function should be Gaussian because the number of the count is normally very high. The width parameter sigma determines the FWHM of any Gaussian through the relation $FWHM = 2.35\sigma$.Is important now to understand which parameters can change the width of the peak of Gaussian distribution sigma.
The minimum detectable by detector is limited by the statistic fluctuation in the charge created, so this is the maximum level of resolution that is possible to achieve. The energy can be absorbed in different way by the detector: by either lattice like creation of phonon or by ionization and than creation of free charge. By the law of energy conservation the sum of the total excitation and ionization must be equal at the initial energy deposited inside the detector.

$$E_0 = N_x E_x + N_i E_i \tag{3.4}$$

where N_x and N_i are respectively the number of excitation and ionization and E_x and E_i are the energies relative at single excitation. In the case of semiconductor E_i is equal to the value of band gap E_g. It's logical assume that, for single event of interaction, there are no fluctuation in the value of the initial energy E_0, and assuming a Gaussian statistic, the formula (previous formula) becomes:

$$E_x \sigma_x = E_i \sigma_i \tag{3.5}$$

where $\sigma_x = \sqrt{N_x}$ and the same for σ_i. Averaging over many events, the variance in the energy allocated in this two type of process must be equal because there is no fluctuation in E_0 . Obviously for doing like a detector only the events of ionization will be important and therefore the fluctuation in the ionization σ_i is the important parameter to determinate the energy resolution of the device.

$$\sigma_i = \frac{E_x}{E_i}\sigma_x \tag{3.6}$$

It's possible to use the formula (la prima formula) to eliminate from N_x:

$$\sigma_i = \frac{E_x}{E_i}\sqrt{\frac{E_0}{E_x} - \frac{E_i}{E_x}N_i} \tag{3.7}$$

N_i is also equal at the number of e-h pair created, so is possible to use the average energy required to create a couple electron and hole $\epsilon_i = \frac{E_0}{N_i}$, putting this formula inside the previous is possible to obtain

$$\sigma_i = \sqrt{\frac{E_0}{\epsilon_i}}\sqrt{\frac{E_x}{E_i}(\frac{\epsilon_i}{E_i} - 1)} \tag{3.8}$$

The second part is called Fano Factor F(reference original articles). Finally the result is that the variance in the number of e-h pair created is not simply the root of the number of pair created but there is a correction constant that considers also the energy loss in the excitation process.
Will exist therefore, for every type of semiconductor detector, a maximum value of resolution due at statistic fluctuation:

$$R = \frac{FWHM}{H_0} = 2.35\frac{\sqrt{N}}{N} = \frac{2.35}{\sqrt{N}} = 2.35\sqrt{\frac{F}{N}} \tag{3.9}$$

Knowing the Fano Factor is possible to calculate, for every incident energy, the maximum achievable resolution. In general also other factors can be contribute to decrease the resolution like noise,drift,defect and therefore the most general formula for the FWHM is:

$$(FWHM)^2_{measured} = (FWHM)^2_{detector} + (FWHM)^2_{statistical} + (FWHM)^2_{noise} + ... \tag{3.10}$$

It is possible for these parameters in some way to reduce their effect. The Fano factor is a statistic parameter and, for this reason, the only way to decrease is to change the material propriety: the ionization energy (band gap energy).

3.4.2 Spatial Resolution

To first order the electrons and holes generated drift along the detector follow the lines of electric field. The drifting time t is simply due to:

$$t = \frac{z}{v} = \frac{z}{\mu E} = \frac{zd}{\mu V_b} \tag{3.11}$$

Where z is the interaction depth,d is the thickness and V_b is the voltage across the device. The longest drifting time is when the interaction depth is d. In reality it must be considered also the thermal diffusion of the carriers during the drifting. This process can increase the volume of the cloud of charge that in the previous discussion was considerate like point. In a simple planar device this effect does not create any problems. But in the presence of different geometries, (strips, pixels, coplanar grid) the size of the cloud can be enough large to create charge sharing between two different electrodes in the same surface. This happens if the pitch between different electrodes on the surface is comparable to the dimension of carriers cloud. It is possible to considerate the distribution of charge, due to diffusion, like Gaussian. The dimension of the cloud is due by the root mean square as:

$$\sigma = \sqrt{2Dt} \tag{3.12}$$

where D is the diffusion coefficient that is linked by mobility by the Einstein relation:

$$D = \frac{kT}{e}\mu \tag{3.13}$$

Using the 3.11 with d as value of interaction depth, the 3.12 becomes:

$$\sigma = \sqrt{2\frac{kT}{e}\frac{d^2}{V_b}} \tag{3.14}$$

the result is independent of mobility and therefore is the same for electrons and holes. For $d = 3000\,\mu m$, $T = 300\,K$ and $V_b = 300\,V$ the transverse diffusion is $\sigma \simeq 40\,\mu m$. The space between the electrodes must be more than this value in order to eliminate every charge sharing contributions.

Chapter IV

CdZnTe

4.1 CZT as Gamma detector

In the wide band gap semiconductor materials CdTe and CdZnTe represents now important material for fabricating room temperature X-ray and gamma-ray detectors. In particular significant effort is still to improve the growth of high resistivity CZT. This material has interesting characteristics that attract the attention of the research:

1. High average atomic number $Z \simeq 50$ (for zinc fraction $x = 0.1$ it is 49) that enhance the Photoelectric effect probability

2. High density that means high quantum efficiency: points 1 and 2 imply high quantum efficiency (4 mm is enough for photons with energy less than 180 KeV)

3. High resistivity (higher than CdTe) imply low leakage current and therefore the use for detecting low energy X-ray (X-ray fluorescence system).

4. Wide band gap (1.572) allows the use at room temperature

5. Good electron transport properties $\mu_e = 1000\ cm^2V^{-1}s^{-1}$ but low hole mobility $\mu_h = 120\ cm^2V^{-1}s^{-1}$

6. The direct band bag permits optical characterizations (as Photoluminescence)

4.1.1 II-VI semiconductors

These compound are normally binary ($CdTe$,$CdZn$) and they are characterized by a II group metal (Zn, Cd and Hg) with a VI group cation (S, Se and Te). In addition also the pseudo binary compound like $Cd_{(1-x)}Mn_xTe$,$Cd_{(1-x)}Se_xTe$ and $Cd_{(1-x)}Zn_xTe$ are common. In fig

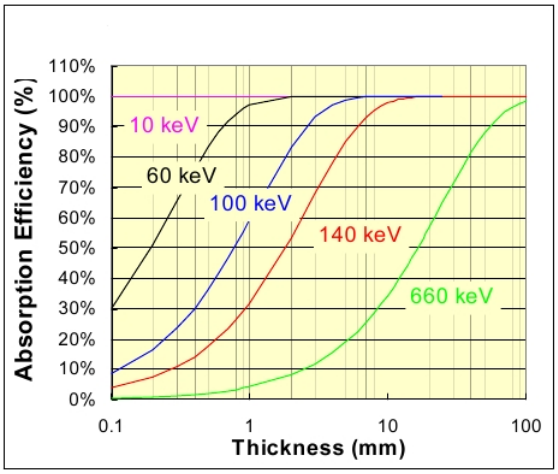

Figure 4.1: Gamma ray absorption in CdZnTe

4.2 it is shown the Band-gap/Lattice constant graph for II-VI semiconductors. It is clearly that these compound are of interest because they show a broad range of bang gap energies: the lowest is 0.15 eV for HgTe and the maximum is 4.4 eV for MgS.

4.1.1.1 $Cd_{(1-x)}Zn_xTe$

As shown in fig 4.2 $Cd_{(1-x)}Zn_xTe$ exists in the line between CdTe and ZnTe where zinc fraction of x varies between 0 and 1. In particular increasing zinc fraction decreases the lattice constant a_o and increases the band gap energy E_g .

$$E_g(x) = 1.51 + 0.606 \cdot x + 0.139 \cdot x^2 \ eV \tag{4.1}$$

The value of band gap is very important for the spectra performance of a detector. Specifically it must be a compromise between two different aspects: an increase of E_g increases the ionization energy and therefore enhance the Fano noise, on the other side this increase can reduce the thermal leakage current and therefore the thermal noise. Adding Zn in CdTe it is possible to increase the band-gap increasing the resistivity of the material. The Adding of Zn has also other benefits like increase in the energy of defects formation [A.W. Webb, S.B. Quadri, E.R. Carpenter, E.F. Skelton, J. Appl. Phys. 61 (1987) 2492.] and enhance the mechanical proprieties of the lattice [J.F. Butler, C.L. Lingren, F.P. Doty, IEEE Trans. Nucl. Sci. NS39 (1992) 605.]. In this work were used crystal of $Cd_{0.9}Zn_{0.1}Te$, that represents the standard composition in all commercial CZT crystals.

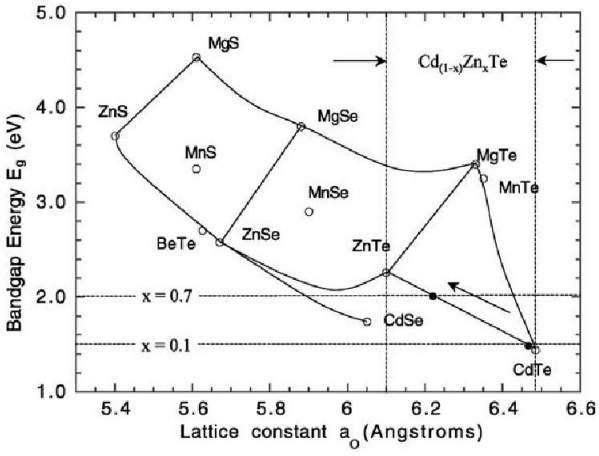

Figure 4.2: band gap of II-VI compound as function of lattice constant [A. Owens, A. Peacock / Nuclear Instruments and Methods in Physics Research A 531 (2004) 18–37]

4.1.2 Transport Property

In General the transport proprieties are important in all type of detector. The complication in CZT is the high resistivity for working at room temperature. This because to grow semi-insulating material implies in all the case addiction of elements to decrease the free carriers. The introduction of defects or impurities can decrease the value of mobility and lifetime. The mobility is, in fact, limited by the scattering between carriers and charged defects. The lifetime instead decrease with the increasing of number of defects either due by trapping and recombination effects. Reduction of lifetime and mobility of the carriers decreases the general resolution of the detector. In order to suppress these defects, the transit time of the carriers t_d must be much smaller than the lifetime of the charges τ. The drift time is given by:

$$t_d = \frac{d}{\mu E} = \frac{d^2}{\mu V} \ll \tau \tag{4.2}$$

where d is the thickness of detector, E and V respectively the electric field and applied voltage. The formula clearly shows that is possible reducing the transit time simply increasing the applied voltage inside the detector (for a fixed thickness). However at the same time the leakage current inside the device increases with voltage and high bias necessarily implies a excessive value of noise. Is important therefore to compromise this two phenomenons for achieve the best resolution. Usually CZT detectors operate with electric field in the range between 1000-2000 V/cm.

4.2 Growth

Chapter V

The Signal

5.1 Signal Formation

A simple planar semiconductor detector is shown in fig 5.1 . It consists in a slab of semiconductor crystal with two metal contacts on two opposite surfaces to form the electrodes. To bias the device a voltage difference is maintained across the two surfaces: in the present

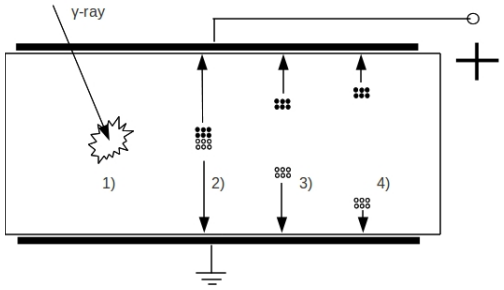

Figure 5.1: Gamma ray interaction and the carriers drifting at different time 1)gamma interaction,2)separation of the carriers,3)drifting,4)collection

case one (bottom) is connected to ground an the top is connected to a positive power supply. Now, suppose that a gamma ray is absorbed by the detector via photoelectric interaction (is possible to consider only this type of process because, as mentioned before, the material for gamma ray detector are designed to interact predominantly via this type of interaction). The effect of the interaction is to create a cloud of electrons and holes that immediately are separated by the applied bias. The electrons drift in the direction of the positive contact and the holes drift in the opposite direction (cathode). Normally, the active layer of the detector are fabricated with high resistivity materials or a depletion area of a diode junction. For this reason the charges created are moving inside a layer without free carriers. The only free charge carriers, other than produced by the incoming radiation, are the charges thermally generated: their drifting form the dark current.

In the case of an active layer constitute by doped semiconductor (or ionic crystal) the situation is different. In this case in fact, after the creation of ehps, the charges generated are immediately shielded by the free charges inside the material. This precisely happens in a duration approximately equal to two or three time the constant called "relaxation time of dielectric"(τ_R). Therefore in this type of material the current signal , due to the ehps created, is observed only when the carriers are collected by electrodes. The opposite happens in the high resistivity materials. In these there are not enough free carries for shielding the charge during the drifting inside the material or, in other words, the drifting is not enough fast. This fact becomes clear from the expression of τ_R :

$$\tau_R = \rho\epsilon \tag{5.1}$$

where ρ is the resistivity of the material and ϵ is its dielectric constant. For a normal sample CZT with a resistivity of $5 \cdot 10^{10}\ \Omega \cdot cm$ and dielectric constant of 11 this product is 49 ms. This value is very long compared to the normal drift time of the electrons ($< 1\ \mu s$) and the holes (1 or 2 μs). This means that the two type of charges , immediately after their separation, can induce signal to the electrodes. The current signal in fact, in contrast to doped semiconductor, is created during the drifting of the charges.
It is possible to explain this induction of signal considering the the system showed in fig 5.2. . In this simple case it is considered a static charged particle q inside the volume of

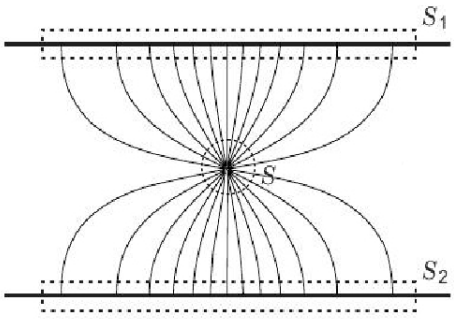

Figure 5.2: Static charge q inside the volume of detector

the detector. The charge , being unshielded, creates an electric field that terminates at the metal electrodes 1 and 2. The result of an integration of this electric field in any Gaussian surface surrounding the charge (for example S) is simply the value of charge q. Now consider the case of a particle exactly in the middle of the two contacts. In this case the integration

is considered over the surfaces S_1 and S_2 surrounding the electrodes 1 and 2. Now in each surface there is only half of the electric field comparing to the case of integration is S, but the number of electric field lines is identical for the two surface and therefore:

$$\oint_{S1} \epsilon E dS_1 = \oint_{S2} \epsilon E dS_2 = -\frac{q}{2} \tag{5.2}$$

there is a minus because the electric field is in opposite verse respect at the normal vector of the surface.
The particle in the middle of the detector induces the same charge in both of the electrodes. It's not difficult to image that q will induce more charge to the nearest electrode but, obviously, the sum over the electrodes will remain in any case q (the modulus). The fact is that this case is very simple and in particular is a static system. Normally it is very difficult to analyze the induced charge continuously. It is easier measuring it's change and, if the two electrodes are connected together like a close circuit, this difference will produce a current. This current is the real signal that is collected.

5.1.1 The effect of trapping in the charge collection

In the real system the crystal is not perfect and normally it contains different type of defects like vacancies, impurity atoms, dislocation, inclusion etc... They can introduce energy states inside the energy gap of the material. These states can trap the carriers and therefore can remove mobile charge available for signal formation. Every moving charge is characterized by a lifetime τ that depends by the amount of defects and by the nature of the carriers (τ_e and τ_h). It represents the time in witch the carriers can survive before trapping or recombination. In general any packet of charge Q_o decays in time as:

$$Q(t) = Q_o e^{-\frac{t}{\tau}} \tag{5.3}$$

It is possible to know the decay in length by replacing t in the previous formula with:

$$t = \frac{x}{v_s} = \frac{x}{\mu E} \tag{5.4}$$

Formula 5.3 becomes:

$$Q(x) = Q_o e^{-\frac{x}{L}} \tag{5.5}$$

where $L = \mu\tau E$ is called drift length. In the case of simple planar geometry this package will induce a charge in the electrode. This amount, for a traveling charge $Q(x)$, for a distance dx is:

$$dQ_i = Q(x)\frac{dx}{d} \tag{5.6}$$

The total induced charge is simply:

$$Q_i = \frac{1}{d}\int_0^d dQ_i = \frac{1}{d^2}\int_0^d Q_o e^{-\frac{x}{L}} dx \tag{5.7}$$

$$Q_i = Q_o \frac{L}{d}(1 - e^{-\frac{d}{L}}) \tag{5.8}$$

As mentioned before the $\mu\tau$ product is different from holes and electrons. Therefore for a charge deposition at coordinate z and with the contribution of electrons and holes the equation 5.8 becomes:

$$\frac{Q_i}{Q_o} = \frac{L_e}{d}[1 - exp(\frac{d-z}{L_e})] + \frac{L_h}{d}[1 - exp(\frac{z}{L_h})] \tag{5.9}$$

where $L_e = \mu_e\tau_e E$ and $L_h = \mu_h\tau_h E$. This expression is called Hecht equation (reference). The only process that can change the signal is the trapping. In reality there is also de-trapping process but, in this treatment, is considerate negligible. It is possible to find an expression for charge collection considering also de-trapping but it is more complicate.

5.1.2 Ramo-Shockley Theorem

The calculation of induced charge on any electrodes due by a moving charge was found independently by Shockley (1938) [] and Ramo (1939) [] in the case of a vacuum tubes (no spatial charges). Later it was proved that the theorem is valid also in system with the presence of stationary spatial charge (Cavalleri et al. 1972). The follow discussion can be applied to all the system in which there is a moving charge that induces charge in the electrodes.
Consider now a general system constitute by: number of electrodes at constant voltage $V_i(i = 1, 2, ...N)$ and specific surface S_i, moving charge q and a spatial static charge $\rho(x)$. For this system the Ramo-Schockley theorem affirms: the charge Q and current induced on a electrode by a moving charge q are:

$$Q = -q\varphi_0(\mathbf{r}) \tag{5.10}$$

$$i = q\bar{v} \cdot \bar{E}_0(\mathbf{r}) \tag{5.11}$$

where q is the value of the charge ($\pm e$) ,$\bar{v}$ is the instantaneous velocity of the charge, $\varphi_0(\mathbf{z})$ and $E_0(\mathbf{z})$ are called respect weighting potential and weighting field. These last two quantity represent the potential and field calculated in the system in the instantaneous position of q (x point) under this conditions: the selected electrode rise at unit potential, all other electrodes grounded and all charge removed ($\rho(\mathbf{r})$ and q). In addiction of the theorem there is also an important corollary: the charge induced is independent of space charge $\rho(\mathbf{r})$ and potential applied on the electrodes. The proof of the theorem is outside the scope of this work but it is possible to find it in the original works [] []. Another interesting review about the Ramo-Shockley Theorem in the semiconductors was done by Z. He [].

5.1.3 Planar geometry

It is possible now apply the Ramo-Shockley theorem to calculate the induced charge in the simplest case of planar electrodes detector(fig 5.1). When a gamma ray is absorbed (photoelectric effect) a large number of ehps are created proportionally to the energy of the photon. Due to the bias (V) the electrons start to drift in the direction of the anode and the hole in the opposite direction: no trapping is considerate now. The output signal will be therefore the sum of these two contributions. The first step is to calculate the weighting potential in the system considering for example the anode like readout electrode. The weighting potential in this case is easy to calculate, in fact it varies linearly in z from the value 0 (cathode surface $z = 0$) to 1 (anode surface $z = 1$) hence:

$$\varphi_0(z) = z \qquad 0 \leq z \leq 1 \tag{5.12}$$

Using 5.10,the total induced charge is:

$$\Delta Q = -(ne)(\varphi(0) - \varphi(Z)) - (-ne)(\varphi(1) - (Z)) \tag{5.13}$$

where n is the number of ehp (no trapping means $n_e = n_h$). By replacing 5.12 into 5.13:

$$\Delta Q = ne \tag{5.14}$$

The expression is very clear: with no trapping the output signal is proportional to the number of ehp generated which is proportional to the incident energy $h\nu$. In the figure 3.3 a) there is

the expected response energy spectra: the amplitude of the signal is always constant and the only fluctuations are due by statistical or electronic noise. Considering again the expression 5.14: this is true only if the integration of the signal is long compared to the drift time of the carriers. In the case of CZT, for example, normally the hole mobility is one order of magnitude less than for electrons and therefore when all the electrons are collected it is possible that the hole are still drifting. In this case the integration of the signal can be less because there is one hole term in the expression 5.13 that can be $\neq 0$:

$$\Delta Q' = -(ne)(\varphi(Z')) + (ne)\varphi(1) \tag{5.15}$$

that means: $\Delta Q' < ne$. Hence it is very important to chose the correct integration time in the way to collect all the charges.
At this point it is necessary introduce the trapping effect in the particular for holes because in the semiconductors for detector application is a very common situation. However, when the hole are strongly trapped, the hole contribution to the signal is negligible and the induced charge becomes from 5.13:

$$\Delta Q \simeq ne(1 - Z) \tag{5.16}$$

Now the charge depends by the interaction position. This quantity is random especially with high energy gamma rays. In this case no spectroscopic information are available under this condition. It is clear that for spectroscopic measure it is necessary to apply some techniques to decrease the contribution due to hole trapping. One of the most used technique is the "single polarity charge sensing" in which the system is sensitive only to one type of charge carriers in this case electrons.

5.1.4 Coplanar-Grid

The incomplete collection of the charges it is a problem also for the gas and liquid ionization detector in which the carries are respectively electrons and positive ions. Due to the difference of mass the mobility of the electrons is bigger that the ions that, therefore, are not normally full collected. For increasing the resolution in this type of detectors was proposed a single polarity technique by Frisch []: the Frisch grid techniques. It consists in a gridded grounded electrode placed in front of the anode inside the detector volume: the distance between the anode and the grid must be smaller than the dimension of the chamber. In this way the anode is electrostatically shielded by the grid: the charges that are drifting in the region

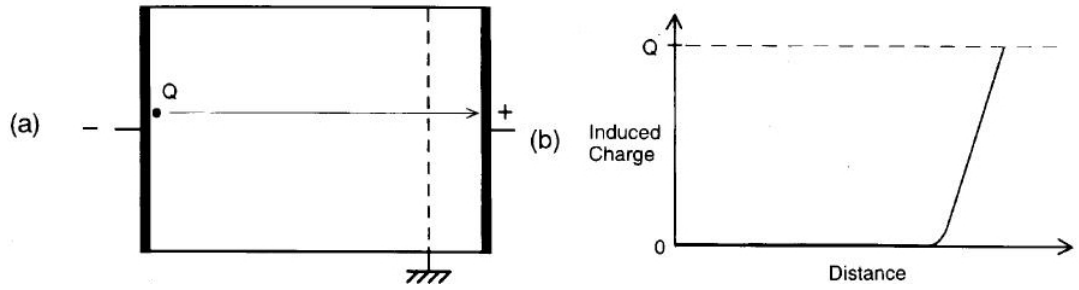

Figure 5.3: a)Frisch grid detector, b) Induced signal due moving charge Q[P.N. Luke, Appl. Phys. Lett. 65 (22), 28 November 1994]

between the cathode and the grid don't create signal to the anode. Only the electrons that pass trough the grid can contribute to the signal. Consequently ,regardless to the collection of positive ions, all electrons created in the region between the cathode and the grid will give always full amplitude signal without any contribution due by ions.
Unfortunately this technique is impossible to achieve in semiconductors detector because it is technologically unable. However it is possible to simulate the behavior of the Frisch grid with a special configuration of the electrodes that was proposed by Luke (1994) called Coplanar Grid technique [P.N. Luke, Appl. Phys. Lett. 65 (22), 28 November 1994], [P.N. Luke, IEEE Transactions on nuclear science, vol 42, no. 4, August 1995]. In figure it is shown the basic structure of the coplanar grid detector. A series of narrow strip electrode

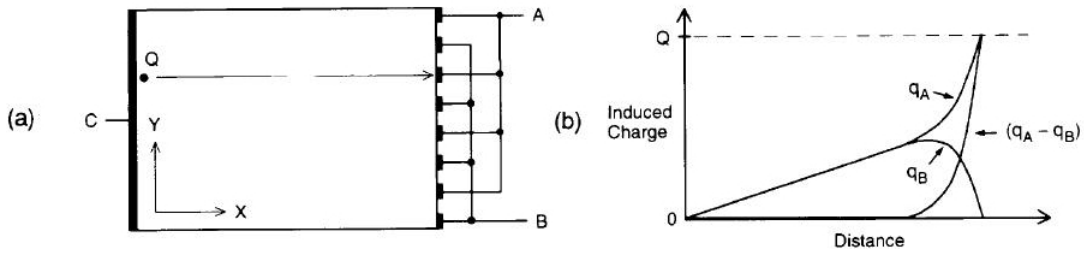

Figure 5.4: a)Coplanar grid detector, b) induced signal in the electrodes A and B[P.N. Luke, Appl. Phys. Lett. 65 (22), 28 November 1994]

(l<<d) are connected together forming two interdigitated grid electrically independent on one surface of the sample (A and B), instead on the opposite side there is a full-area electrode (C). Supposing now the case in which the two grids are at the same potential (ground) and C at high bias$-V_c$, assuming also to measure the signal from electrode A. The strips are

at relative positive bias for collecting the electrons because in the semiconductor must be eliminate the contribution of holes. The induced signal as shown before depends only by the weighting potential that in this case is shown in fig 5.5. The boundary condition for calculation are: A at unit potential, B and C grounded and removing all the charges. The

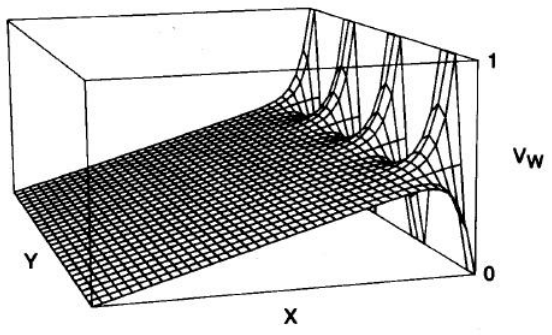

Figure 5.5: Weighting field calculated for coplanar detector of figure () assuming the electrode A as collecting[P.N. Luke, Appl. Phys. Lett. 65 (22), 28 November 1994]

shape of the induced charge Δq in A and B can be easily obtain by projecting the path of the charges on the weighting potential surface of fig 5.5.

$$\Delta q = Q\,\Delta\varphi(z) \tag{5.17}$$

where Q is the charge of the carrier and $\Delta\varphi(z)$ is the change in the wp along the distance z. It is possible to recognize in this picture two different zone: Far-grid region and a Near-grid region [M Amman, PN Luke - Nuclear Science Symposium, 1998]. In the first region the weighting potential of the two grid is the same and therefore the moving particle induces the same charge in both of electrodes. The induced charge in the two electrodes A and B is shown in fig 5.4 b). It is only in a small region close to the anode (near-grid region) that the weighting potential of A rapidly increases to 1 and these of B decreases to zero.
Consider now a new signal given by the subtraction of the signals of the two electrodes A and B ($q_A - q_B$). This new signal has the peculiarity of being zero along all the Far-grid region while it rises from 0 to Q rapidly in the Near-grid region. Consequently the difference of A and B signals a new signal is obtained that is analogous to the induced charge in the Frisch grid configuration fig 5.3 b) and 5.4 b).
The shape of weighting potential for the electrode B is identical to that of A except for the

fact that the potentials, at the anode surface, are interchanged. In the normal configuration a slightly different bias is maintained between two grids: in this way all the charge are collected by only one of the two grids called collecting grid (cg). The other grid is labeled as non collecting grid (ncg).

It is possible to understand the physical behavior of the system imaging the electrostatic field flux line that start from the charge and terminate at the electrodes. When the charge is far from the anode (in the far-grid region) the lines are distributed uniformly between the cg and ncg strips because they are interdigitated with identical dimension and shape. When the particle is in the near-grid region the density of the flux lines on one strip surface rapidly change for every small change in the charge position. In particular the number of lines increase in time in the collecting strip at the expense of all other strips. It is only in this small region that the two signal start to be different: the signal of the cg rises to Q and ncg signal fall down at zero.

In this point of view it is clear that the two grid must be identical, symmetrical and with a high degree of interdigitation in the way to have the same induction charge onto when the charge is far from the anode. Another important parameters is the dimension of the near-grid region that is the analogous of the distance grid-to-anode in the Frisch detector. This region must be small as possible because only the events of interaction that happen outside this region are with single polarity sensitive. By decreasing the pitch among strips (or increasing the number of the strips) the size of near-grid region can be reduce with increasing in the number of position independent events. On the other side it is important to keep a voltage between the grids (V_g) high enough to have no shared charge among the cg and ncg. Otherwise the signal amplitudes will be reduced by sharing charge between the electrodes. The choice of V_g must take into account also the noise due to the leakage current between the grids: too high voltage could mean dominance of noise and too low voltage could mean very low collection efficiency (high sharing charge events).But the reduction in the pitch size means reduction in the resistance between the two electrodes (cg and ngc) and consequently a reduction in the voltage among grids must be done to decrease the noise. Consequently, as said before, it implies a reduction in collection efficiency due to reduction in V_g. Finally the pitch should be small compared to the thickness of the detector but enough big to allow high value of V_g without high noise contribution.

The coplanar grid method provides also other two additional features in addition to single polarity sensing (remove the hole trapping effect). One of these is the ability to correct the electron trapping effect. In general in fact also the electrons are trapped inside the crystal

and, trough much less than the hole, this effect can affect the energy resolution of the system. The other important feature is the possibility to obtain the position of interaction information directly from the signal.

5.1.4.1 Resolution

The vast improvement in the spectra resolution obtained using this technique in CdZnTe was proved at first by Luke [][][] : in particular coplanar grid provides an effective method to eliminate the effect of poor hole mobility in the CZT detector. In the original work of Luke a resolution of 3.7% at the 662 KeV peak of^{137}Cs was found for a $5\,mm^3$ CZT detector. During the last years big effort were done to improve the maximum resolution achieve by this type of detector and now a normal resolution less than 2% is available for a typical $1\,cm^3$ commercial detector for the same peak of ^{137}Cs. In particular strong effort were done to optimize the geometry in the coplanar grid contact in the way to optimize the uniformity of the weighting potential along the radial coordinate of the crystal. A fundamental work were done by Z. He et al. [] and by M. Amman (and P.N.Luke) [] to purpose good geometry of contact.

5.2 The Signal Acquisition

The signal charge, provided by detector, can be quite small ($5 \cdot 10^{-17}$ C for 1 KeV x-ray), so the signal must be amplified to be measured and processed for spectroscopic proposes. In general, as will be showed later, in a normal measure system there are more than one amplifier. in this chapter it is showed the first of this amplifier that is connected immediately later the detector and it is called "preamplifier". In general it's possible to categorize these amplifier systems into three general modes of operation: current mode, mean square voltage mode and pulse mode. The current mode is used when event rates are very high because in this operating mode the system is sensible only to the fluctuation of the average current value. The mean square voltage mode is normally used in the reactor instrumentation because it is useful in enhancing the relative response to large amplitude events. Most applications are better served by recording every information about amplitude and timing of individual events and this is possible only in the pulse mode; such application are generally called radiation spectroscopy. The nature of the signal pulse (produced by single event) depends on the input circuit between the detector and the amplifier, the equivalent circuit can be often represented in fig**??** . The detector signal is a current pulse amplitude i_s and duration t_c(provided by current supply) in parallel with a capacitance C_d (capacitance of the detector)

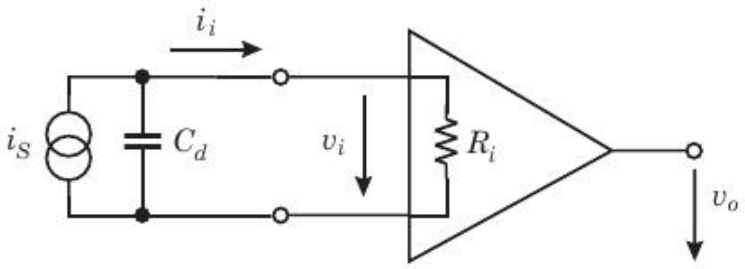

Figure 5.6: Pulse mode simplified circuit[1]

and a resistance R_i (in general it's a general resistance of the circuit) the signal charge is:

$$Q_s = \int i_s(t)dt \tag{5.18}$$

The voltage at the output of amplifier in general depend proportionally on the input voltage, and the proportional constant is simple the gain of the amplifier.

$$v_o = -A \cdot v_i \tag{5.19}$$

Since the i_s changes with time (t_c during the pulse length) it is possible to identify two separate extreme mode of operation that depends on the ratio of t_c and the time constant of the system $RC = \tau$.

- Small RC ($\tau \ll t_c$)

In this case the time constant of the system is smaller compared with the collection time, and the output signal voltage has essentially the same time-dependence of the current produced by detector.

- Large RC ($\tau \gg t_c$)

In the real system it is more probable that the constant RC is larger compared to the collecting time and therefore the response of the system is slow compared to the changing time of the signal. This is due to detector capacitance that discharge slowly with exponential function governed by time constant τ.

$$v_o = V_o exp(-t/\tau) \tag{5.20}$$

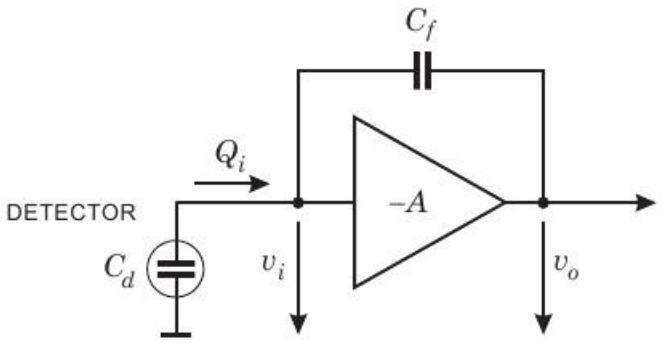

Figure 5.7: Scheme of a charge-sensitive amplifier[1]

The main information in the spectroscopic measure is the am mount of ehps created by single interaction. In the case of small RC this is trivial because the response of the system is identical to the created signal. Fortunately also in the case of large RC this information is not lost. In fact the maximum value of the voltage V_o depends only on the amount of charge deposited in the detection volume in the way:

$$V_o = \frac{Q_s}{C_s} \propto \int i_s(t)dt \tag{5.21}$$

Where Q_s is the value of created charge. Even the amplified signal is not exactly like the real signal (due to the delay time of response), the physical information is inherently contained. The signal of two systems discussed before (small and large RC) is showed in fig (figure 109 knoll).

In the pulse mode this preamplifier normally works with a feedback capacitance (C_f) in the manner called "charge-sensitive amplifier",it is showed in fig 5.2. The basic building block is an inverting voltage pre-amplifier (doesn't change with a positive pre-ampl.) with a high input resistance that for simplicity considerate infinite. Since the amplifier inverts, the gain is $v_o = -A \cdot v_i$. The voltage across the feedback capacitor

$$v_f = v_i - v_o = (A+1)v_i \tag{5.22}$$

$$Q_f = C_f v_f = C_f(A+1)v_i \tag{5.23}$$

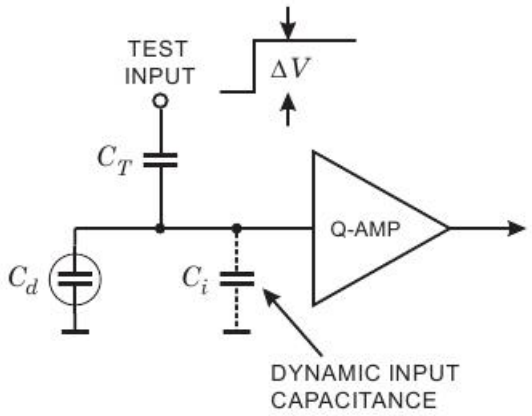

Figure 5.8: Calibration of a charge-sensitive amplifier[1]

Since no current flow thought the amplifier, all the signal current must charge up the capacitance to $Q_f = Q_i$. So the input capacitance appears like a "dynamic capacitance":

$$C_i = \frac{Q_i}{v_i} = C_f(A+1) \tag{5.24}$$

The voltage input per unit of input charge is:

$$A_Q = \frac{v_o}{Q_i} = \frac{A \cdot v_i}{C_i \cdot v_i} = \frac{A}{C_i} = \frac{A}{A+1} \cdot \frac{1}{C_f} \simeq \frac{1}{C_f} \qquad (A \gg 1) \tag{5.25}$$

so the the charge gain is controlled by a component, the feedback capacitor. The signal charge is distributed between the detector and the dynamic input capacitance, the ratio of measured charge and signal charge

$$\frac{Q_i}{Q_s} = \frac{C_i}{C_d + C_i} = \frac{1}{1 + \frac{C_d}{C_i}} \tag{5.26}$$

The input capacitance must be larger compared with the detector capacitance. Another useful feature of this type of configuration is the ease of charge calibration. It is possible to test the amplifier by adding a test capacitor as show in Fig5.2. A voltage step injects a well-controlled amount of charge into the input and , if the input capacitance is enough large, the ΔV will be applied nearly completely across the test capacitance C_T and in the

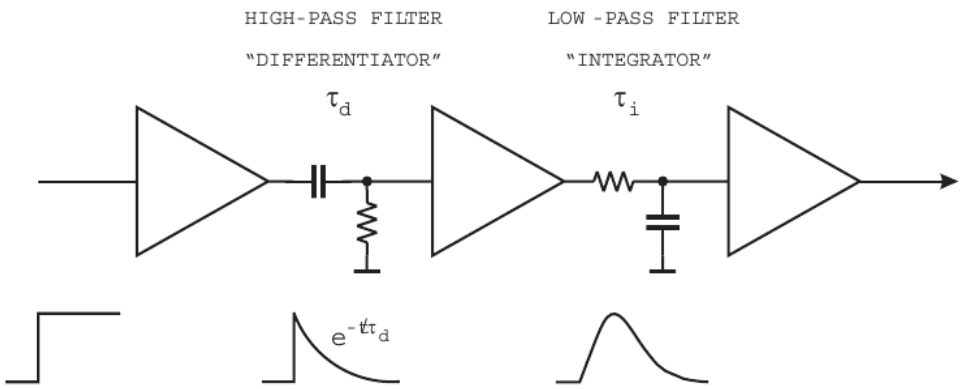

Figure 5.9: A simplified scheme of the shape amplifier

input will be an amount of charge equal to $\Delta V \cdot C_T$.

$$Q_T = \frac{C_T}{1 + \frac{C_T}{C_i + C_d}} \cdot \Delta V \approx C_T \cdot \left(1 - \frac{C_T}{C_i + C_d}\right) \cdot \Delta V \approx C_T \cdot \Delta V \qquad (C_i \gg C_d, C_T) \qquad (5.27)$$

so the system can be calibrated with the detector connected.

5.3 Signal Processing

To improve the signal amplitude and time resolution, the detector signal must be processed. This processing changes also the shape of the signal and hence sometimes the signal processing is also called pulse shaping. The simplest pulse shape is shown in fig . The input of this system is the signal of preamplifier that is shown like a square-wave with an infinite duration. It is only an approximation of the real signal (fig knoll) as the decay time is long compared to the signal rise time. In general it's possible to simplify the system into two principal parts:

- High Pass Filter (CR Circuit). It is also called "differentiate" because, if the potential drop on resistor is very small compared to that on the capacitor, the output signal is the time derivative of the input signal. This filter introduces a decay time constant τ_d.

- Low Pass Filter (RC Circuit). It is also called "integrator" because the output signal is the time integration of the input. This circuit also introduce a time constant but in this case it's a rising-time constant.

The behavior of the general system is simple if the response function of the two circuit is considered. The frequency response is the product of the single response of each component:

$$G(f) = G_{diff}(f) \times G_{int}(f) \tag{5.28}$$

Using the Laplace transformation the product becomes the convolution:

$$g(t) = g_{diff}(t) * g_{int}(t) \qquad V_{out}(t) = V_{int}(t) * g_{diff}(t) * g_{int}(t) \tag{5.29}$$

If it is possible to suppose a unit signal in input (for examples 1 V) the 1.12 becomes:

$$V_{out}(t) = \frac{\tau_d}{\tau_d - \tau_i}(exp^{-\frac{t}{\tau_d}} - exp^{-\frac{t}{\tau_i}}) \tag{5.30}$$

where τ_d and τ_i are the differentiate and integrator time constants.
The simplest form of 1.13 is when $\tau_d = \tau_i = \tau$.

$$V_{out}(t) = (\frac{t}{\tau})exp^{\frac{t}{-\tau}} \tag{5.31}$$

That means that the signal is Gaussian and therefore symmetric. Changing the two relative constants τ_d and τ_i can change the shape of the output signal. In same amplifier is possible to change with two regulators the value of this parameters.

Chapter VI

Experimental Setup

Detector system general in this part will be explained the general detector system, general overview and a simple description of every components of the system. In chapter 7 it will show the scheme of each measure system in detail.

6.1 Detector

This is the sensor that convert the energy deposited by a particle in a electrical signal: in the case of semiconductor this can be achieved by a creation of a large number of ehps. The number of e-h pair is connected to the energy of the particle and so, by integrating of the signal, it is possible to obtain the nature of every event of interaction. This signal is also very short time (ns) and the spatial cloud of the charge is order of μm, for thus reasons this type of detector can manage a very high particles rates.

6.1.1 Detector Preparation

Two detector were made onto two crystal of $Cd_{0.9}Zn_{0.1}Te$ growth with boron oxide encapsulate vertical Brigman technique in IMEM institute. The samples are labeled as 024-01 and 032-02, the names are different because the samples were cut by two different ingots. For this reason it is possible that the properties can be different. The dimension of the samples were:

- 024-01 $10x10x(2.95 \pm 0.01)\ mm^3$.
- 032-02 $10x10x(2.89 \pm 0.01)\ mm^3$.

In this project were done all the part of the detector processing, in order: lapping, cleaning, contacts preparation, passivation and bounding.

6.1.1.1 Surface Preparation

In order to reduce surface roughness, and also allow good adhesion of the metal contact, the surface was prepared using a standard procedure that involved mechanical polishing of the sample (lapping). The machine used in this work was a UNIPOL 810 Polishing/lapping machine (MTI corporation) that is shown in Appendix B. The procedure involved a constant rotation of the plate at 20-30 rpm and Al_2O_3 powder of two different size:

- 1 h with 0.5 um diameter powder dispersed in Ethanol Diol
- 1 h with 0.05 μm diameter powder dispersed in Ethanol Diol

After mechanical polishing, to produce a defect free surface, and also reduce the damage caused by lapping, ingot slicing and dicing, is normally necessary to chemically etch the surface. The most common chemical etchant is 2% Bromine in methanol. In particular the standard time of the etching is 120 sec. The sample 032-02 was processed in this common way.
Sometimes the etching in BrMeOH can produce in the surface a corrugate layer called "orange peel". This was the case of the sample 024-01. Therefore the sample was lapped again and processed the second time without chemical etching. In this way was possible to compare the detector response for two different processes.
After lapping and chemical etching is required a final chemical cleaning in order to remove all unwanted substances. The sample was washed with 2 minutes immersion in Isopropanol, 2 min. in Methanol and 2 min in Acetone all at room temperature. The mechanical polishing creates in the sample one Te-rich surface in the crystal. The exposure of this surface to air can produce a oxide layer (TeO_2) that can change the behavior of the electric contacts. But, according to [1], the thickness of the TeO_2 layer after three days in air (the time between lapping and contact creation) is approximately around 0.4 nm, less than what is required to change significantly the electrical properties of the contacts.

6.1.1.2 Contact Preparation

In order to create a coplanar grid device it's necessary to create two independent interdigitated grids. The complexity of this geometry requires the use of photolithography. In this work the photolithography process was also used for the planar contact in order to increase the accuracy of the contact shape and again in the passivation process. The complete lift-off

process is explained in appendix A. In fig. 6.1 it is possible to see the dimension of the contacts and their relative geometry. In particular the contacts were been fabricated with

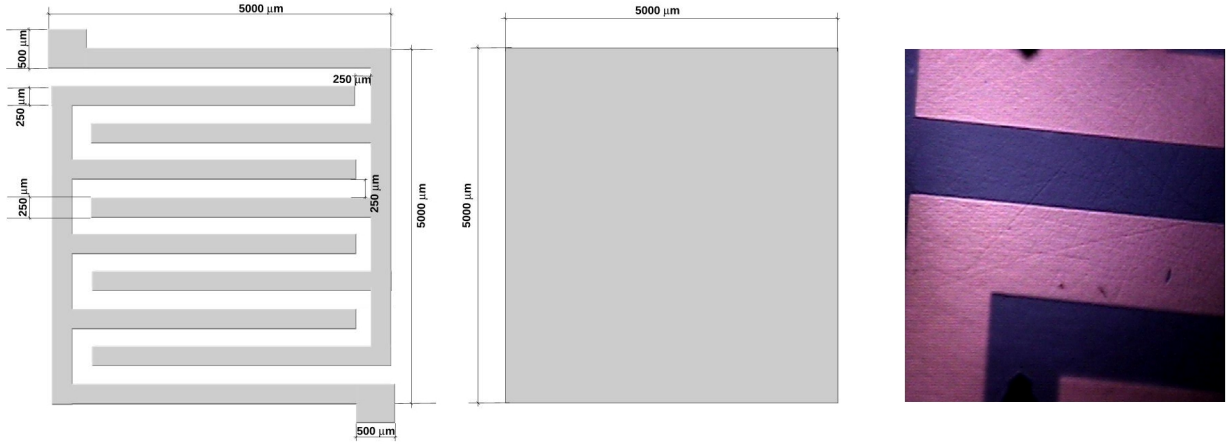

Figure 6.1: Size and geometry of the contacts

sputtered Platinum (99.999%) with a Emitech K575X (Details in Appendix B). Thickness was 80 nm in all the contacts. The current on target was set at 20 mA which corresponds a rate of 25 nm/min: in this operating condition the grain size is less than 5 nm [Emitech website]. The mask aligner was a Karl Suss MJB-3 Mask Aligner (image in Appendix B).

6.1.1.3 Passivation Process

As mentioned before the chemical etching can create on the surface of the sample a Te-rich layer. This non stoichiometric part of the crystal has a higher electrical conductivity in comparison to the bulk. Lower resistivity means increasing in the leakage current and therefore an increase in the noise of the device. While the bulk resistance is very high the surface resistance can be lower and, since they are electrically in parallel, it is possible that the resulting resistance between the electrodes can be lower that predicted. To reduce this problem an oxide layer was created on the whole surface of the sample after contact deposition.The passivated layer was created by immersion the sample in 20% H_2O_2 solution for 2 minutes and a consequent rinsing 2 minutes in acetone. Before this process was deposited a layer of photoresist above the metal contact area in order to reduce the damage caused by the solution. The measures of surface resistance (chapter 7) shown the real effect of the passivation process in order to enhance the surface resistance.

6.1.1.4 Pcboard and metal box

The finished detector was mounted on a pcboard designed by Radiation Laboratory (University of Surrey). The cathode was contacted with silver paint in the way to make electric contact between full area electrode and the pcboard. The two grids were bounded to the pcboard contacts with a wire bonding with a Au wire ($25\,\mu m$ diameter). But, in this case, the wire bonder was working without ultrasonic soldering. This because the ultrasonic can destroy the crystal lattice under the contact and changing the electrical properties of the contacts. For eliminating this problem was used a 2 components epoxy glue for bonding the wire to the Platinum contacts. The detector bounded was mounted inside a aluminum box

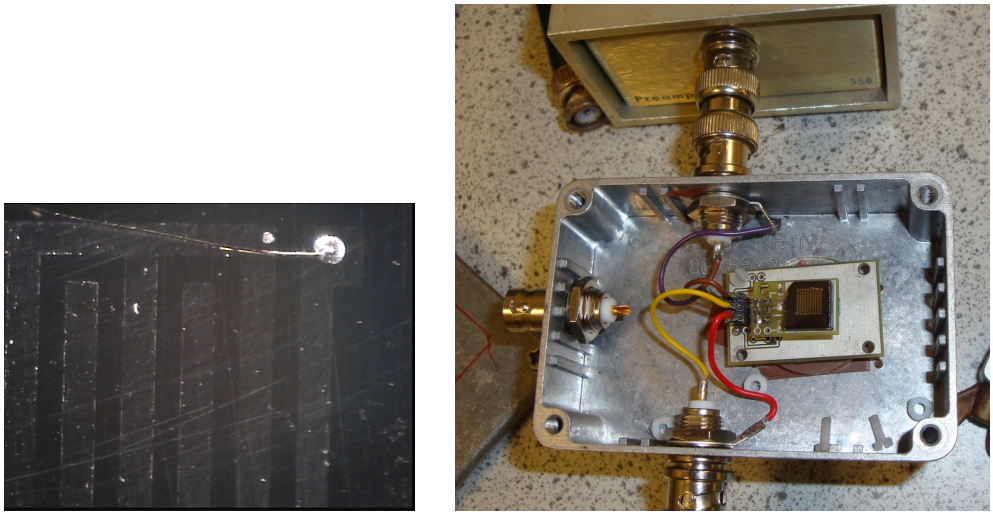

Figure 6.2: On the right side the photograph that shows the wire bounded by glue on the electrode surface. The left figure shows the detector mounted inside the metal box and connected to the preamplifier.

connected to amplifiers by two BNS connectors as shown in fig. 6.2 (right).

6.2 Preamplifier

The behavior of preamplifier is to increase the height of the signal (that can be very small) and to decreases the noise that afflicts the signal. As will see later the most important parameters for designing a good preamplifier is the value of the total capacitance in parallel with the input.

6.3 Amplifier

The shaping amplifier (pulse shape) is very important to improve the ration signal to noise, the basic idea is to eliminate the contribution of the noise by applying a filter that change the frequencies response to favor the signal and decrease the noise level. Another feature of the shape pulse is that permits to introduce a fixed decay time and a rise time for every pulse signal in the way of decrease the total pulse width. Reducing the size of the signal is important to eliminate the pile-up of two consecutive pulse otherwise would be a wrong measure of the amplitude of the second peak.

6.4 Multichannel analyzers (MCA)

A multichannel analyzer (MCA) is a device composed of many (usually between 256 and 8K) single channel analyzers (SCA). A single channel analyzer is a logic device (0/1) that compares a 0-10 volt unipolar voltage pulse to a preset voltage range. If the input signal is between the voltage range the SCA output will be yes(1) otherwise no(0). The SCA output is then sent to a counter which incremented every time the SCA provided a positive pulse. When a string of SCAs and counters are connected such that the voltage regions of the SCAs are continuous (e.g. [4.0,5.0), [5.0, 6.0), [6.0,7.0), etc.) then the result an MCA which converts a series of voltage inputs into a voltage histogram. It is very important note that MCA works with voltage and not with energy. For this reason for each measure it must required the calibration of the system.
In addition at the input connector it is common another connector called Gate. Tt this entry it is possible to connect a source of signal to allow on of the three working mode of MCA: normal mode (gate off), Coincidence or Non-Coincidence. In these last two cases the counter increase or not (respectively) if in the gate there is a positive pulse signal. In this way it is possible to record (or discriminate) only the signal desired. Finally the MCA is connected with a computer and a software that plots the voltage histogram for each measurement.

6.5 Calibration Procedure

The calibration of the system is very important to quantify the energy that the detector is measuring. This is possible comparing the MCA peak centroid with a well defined quantity of energy in the input of the system. The process is to measure some values of this two quantity (channel number and energy input) in the way to extrapolate a law that, generally,

is linear. The general scheme of calibration is shown in fig. 6.3 . It's very similar to a

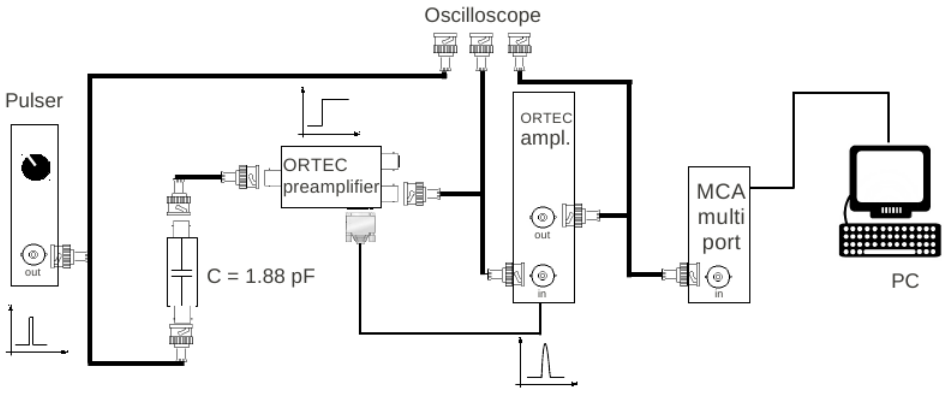

Figure 6.3: Generic scheme of the calibration system:

system for spectroscopic measure the only difference is that the detector is substituted by a pulse supply connected to a capacitor. In this way is possible to simulate the behavior of the detector but with a well defined energy deposited.
As is shown in fig 6.3 a pulse of height V_{pulser} goes from the pulse to a capacitance C_{test} . The quantity of charge will be therefore:

$$Q_{pulser} = V_{pulser} \cdot C_{test} \tag{6.1}$$

However in the detector are created electron-hole pairs (ehp) due to interaction with particles or radiation. Is this number, for single interaction event, that permits to calculate the energy of interacted particle or quanta. Obviously this is true if is known the value of energy required for the creation of one e-h pair W. According to above it is possible convert the quantity of charge in number of ehp:

$$ehp = \frac{Q_{pulser}}{e} \tag{6.2}$$

where e is the charge of electron ($1.602 \cdot 10^{-19}\ C$).
Now it is easy to calculate the energy as:

$$E_{pulser} = W \cdot ehp \tag{6.3}$$

In this project it was used for calibration the value of $W = 4.64$ (eV/ehp) [A. Owens, A. Peacock / Nuclear Instruments and Methods in Physics Research A 531 (2004) 18–37] and

the value of the capacitance was in all the calibration the same $C_{test} = 1.88\ pF$.

Chapter VII

Experimental Result

7.1 IV characteristic

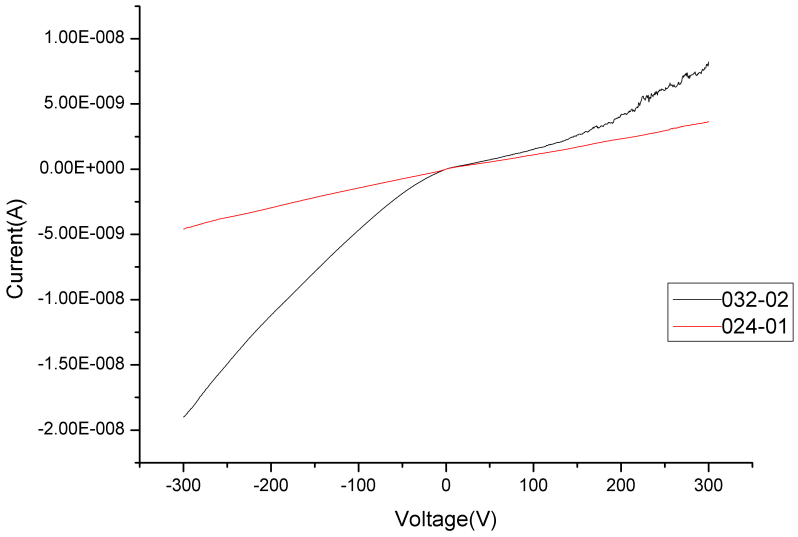

Figure 7.1: IV characteristic of both the samples

In fig. 7.1 it is shown the IV characteristic for both device. In this measure the two grid were connected together to simulate a simple two contacts device. A KEITHLEY 487 Picoammeter/Voltage source was connected to the device. It provided the voltage (BNS cable) and, for each value, it was recording the value of current (TRIAX cable). A LabView program was controlling all the parameters of the measurement in particular: the voltage step, the number of current value measured for each step and the time distance between two consecutive current measure. This last parameter is very important because, in the way to

measure the real current in the detector, it must required keep enough time to eliminate all the inertial effect in the system.
The IV characteristic show different behavior for the two detectors in particular the 024 exhibits higher resistivity. The value of resistivity is standard calculated by the liner fit in the low voltage region (-1 V to 1 V). It was also measured the surface resistance between the two grids. In this case the voltage and the current were measured between the two grid contacts while the full area contact was connected to ground. Also in this case the value of resistance is simply the inverse of the slope in the linear fitting. One last detail was the resistance ($1K\Omega$) connected serially to one electrode in order to reduce the possible damage due to high current. (figure Resistance bulk

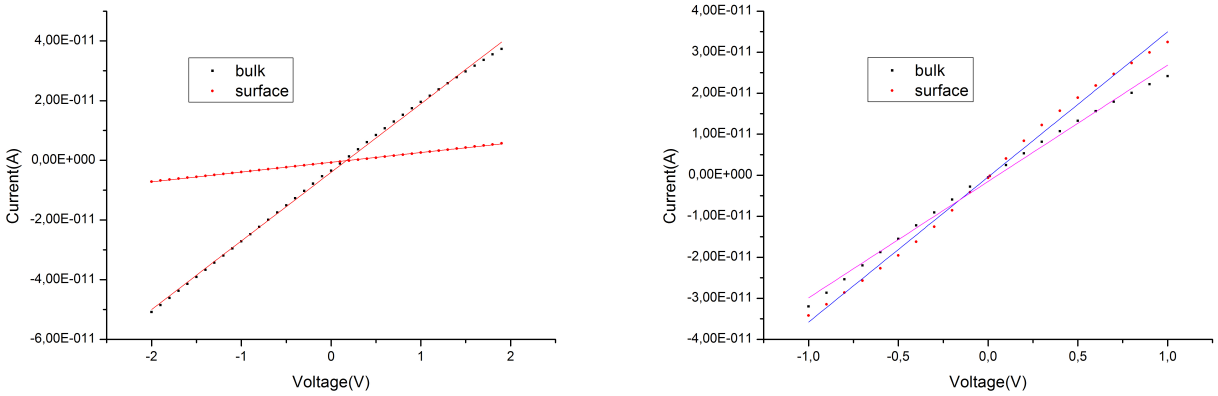

Figure 7.2: Linear fitting of IV characteristic: left 024-01 right 032-02

Sample	Bulk resistance (Ω)	Surface resistance (Ω)
024-01	$4.4 \cdot 10^{10}$	$3.1 \cdot 10^{11}$
032-02	$3.5 \cdot 10^{10}$	$2.8 \cdot 10^{10}$

Table 7.1: Resistance values for the two samples

7.2 Transport Properties

The transport properties of the crystal are a crucial parameter for the final quality of the detector, in particular the value of mobility (μ) and lifetime (τ) are the parameters of interest.

These study can be done by creating a well know quantity of free carriers inside the material and study their moving. For creating free charge it can be used different type of sources: in this this in the transport measure were used always alpha particles. These particles have two important features: as mentioned in the 1th chapter, they are mono energetic and therefore it is knew exactly the quantity of energy deposited. The other feature is that all the ehps are created very close (few μm) affected detector area. Consequently one type of charge is collected immediately by one electrode and its contribution at the signal is:

$$\Delta q = Q\,\Delta\varphi(z) \tag{7.1}$$

but in this case $\Delta\varphi(z) \to 0$ due to the small distance crossed by charges. The result is that the induced signal is predominantly due to single carrier transport: the opposite charge in fact travels all the thickness of the device. In this way is possible to measure separately the transport properties of electrons and holes.
The strong interaction between alpha particles and matter forced to use the vacuum for reducing the attenuation due to the air. Therefore the device and the source were mounted inside a special metal box connected to a vacuum rotating pump (maximum vacuum $6 \cdot 10^{-2}$ Torr). In this type of experiment the Coplanar grid configuration is not required because the transport properties are a bulk characteristic, it is required a simple planar device. This simple configuration was done connecting together the two grids as a only one electrode.
In all the transport measurement it was used as alpha source ^{241}Am S37.RG.

7.3 Measure of $\mu\tau$

In figure 7.3 is shown the system for measuring the $\mu\tau$ product. As is shown in figure the power supply was connected to the two grid (top), the source was collocated above the same side (top) and the planar contact (bottom) was connected to the ground (metal box). Finally the signal was token from the top contact.
In this configuration, negative power supply was meaning signal from electrons and positive supply signal from holes. The mono energetic nature of the alpha particles permits to evaluate how many charges are created for each interaction by relation:

$$Q_0 = \frac{E_\alpha}{W} q \tag{7.2}$$

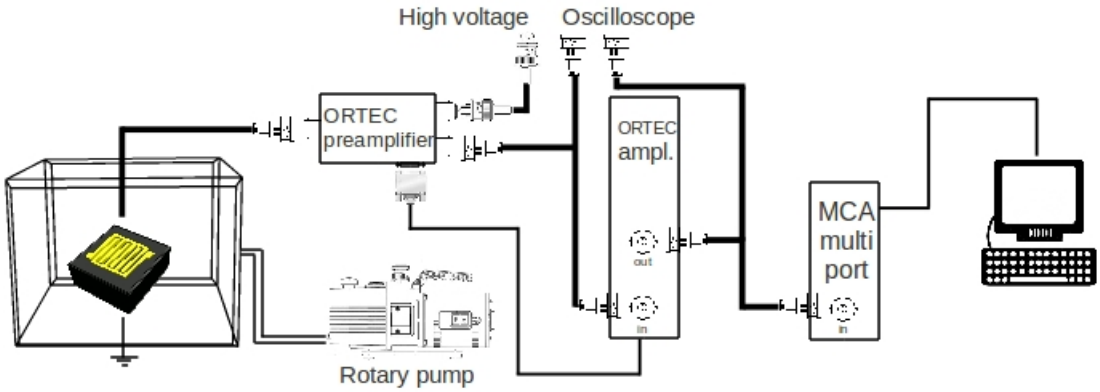

Figure 7.3: System for $\mu\tau$ calculation: Preamplifier ORTEC 142 IH, Amplifier ORTEC 570 and a MCA Multiport II (Canberra)

where Q_0 is the charge produced by the radiation interaction, $E_\alpha$is the energy of alpha particles and W is the energy required for creating one ehp. It is possible therefore to evaluated how many charges are collected by the system. The ratio between the real and measured charges is called Charge Collection Efficiency (CCE) and it is a parameter about the efficiency of collection of the system.

$$CCE = \frac{Q}{Q_0} \tag{7.3}$$

where Q is the charge collected (at fixed V) and Q_0 is the charges produced by the radiation interaction. It is also possible to compare directly the energy of alpha and the energy E at the output of MCA:

$$CCE = \frac{Q}{Q_0} = \frac{\frac{Eq}{W}}{\frac{E_\alpha q}{W}} = \frac{E}{E_\alpha} \tag{7.4}$$

In general this quantity can vary in function of the voltage applied to the detector trough carriers trapping (chapter 4, section 4.1.2). For a single carrier this behavior is described by the Hecht equation (formula 5.9). In this case the thickness of detector is very big compared with the interaction depth and, for this reason, in the equation this last quantity can be neglect.

$$CCE = \frac{\lambda}{d}[1 - e^{\frac{d}{\lambda}}] \tag{7.5}$$

The quantity λ is called carrier drift length and is equal to:

$$\lambda = \mu\tau E = \mu\tau \frac{V}{d} \tag{7.6}$$

The fitting with Hecht equation permits to extrapolate the quantity $\mu\tau$ separately for electrons and holes.
Like alpha source was used the source S037.RG ^{241}Am. The parameters of the amplifier was set in different way for electrons and hole: the shaping time of the amplifier was $3\mu s$ for the electrons and $6\mu s$ for holes.

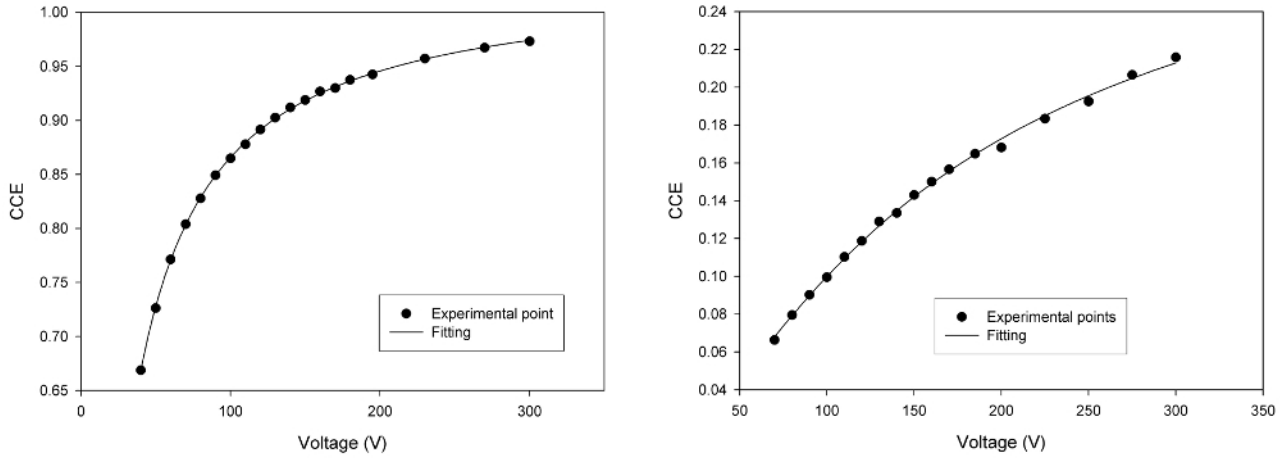

Figure 7.4: Measure of $\mu\tau$ in the sample 024-01 left electrons and right holes

The measure and the relative fitting for the two sample are shown in figures 7.4 and 7.5. The fitting was done with a function similar to equation (number) with some unfixed multiply constant. Every point in the graph represents the peak position of alpha spectra at difference bias. Every peak was fitted with a Gaussian with program $Origin^{(R)}$ to extrapolate the peak centroid position. The result of the fitting shown a very good $\mu\tau$ product that is comparable with commercial values [Peackoc reference]. In particular the value measured in both of the samples for the holes is particular high compared with measure of $\mu\tau$ done in sample of the same ingot.

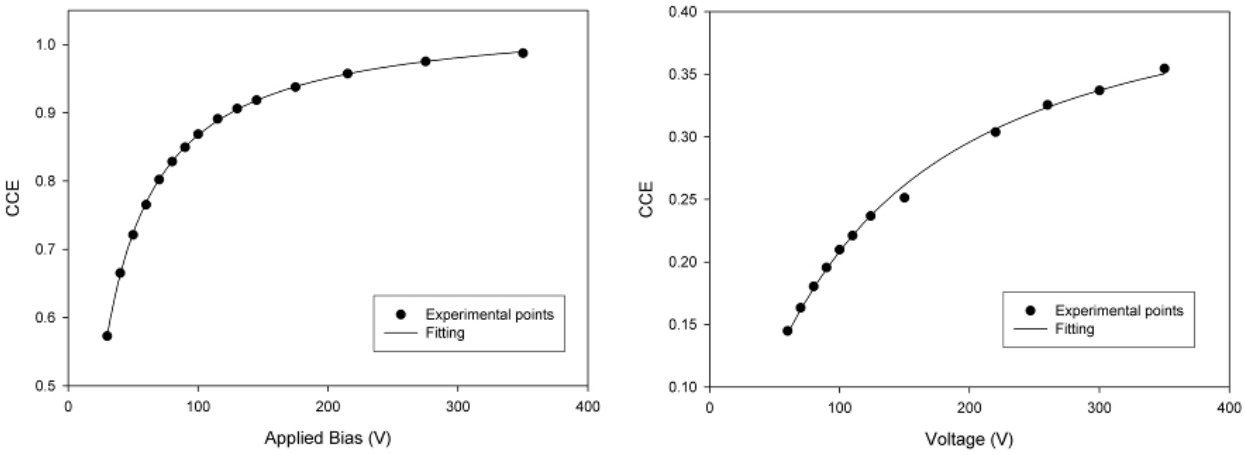

Figure 7.5: Measure of $\mu\tau$ in the sample 032-02 left electrons and right holes

7.4 Time Of Flight (TOF)

The time of flight is the dynamic measure of the drift time t_d of the carries. This is possible with the valuation of the rising time of every pulses signal. The drifting velocity depends on the value of mobility as:

$$v_d = \mu \cdot E = \mu \cdot \frac{V}{d} \tag{7.7}$$

for crossing the detector of thickness d, with an applied voltage V, the charge spends a time τ, this is simply the raising time of the signal. Therefore:

$$\frac{d}{\tau} = v_d = \mu \frac{V}{d} \quad \rightarrow \quad \mu = \frac{d^2}{V}\frac{1}{\tau} \tag{7.8}$$

By plotting the inverse of the rising time (τ^{-1}) with $\frac{V}{d^2}$ it is possible to extract the value of μ directly as the linear coefficient of the linear fit. The system of measure is shown in fig. 7.6 . The time filter amplifier was used only for inverting the signal because the Constant fraction disk (CFD) work only with positive input. For electrons there are no problem but the signal of holes is negative and therefore was required an inverting component. The Constant fraction was connected to the gate of MCA and it generated a square signal for each pulse coming from preamplifier. In this mode the square pulse identified every single pulse so as to record them one by one. The results for the two samples are shown in fig 7.7. For every voltage a program (labVIEW) recorded 4000 pulse signal and for each one it calculated the

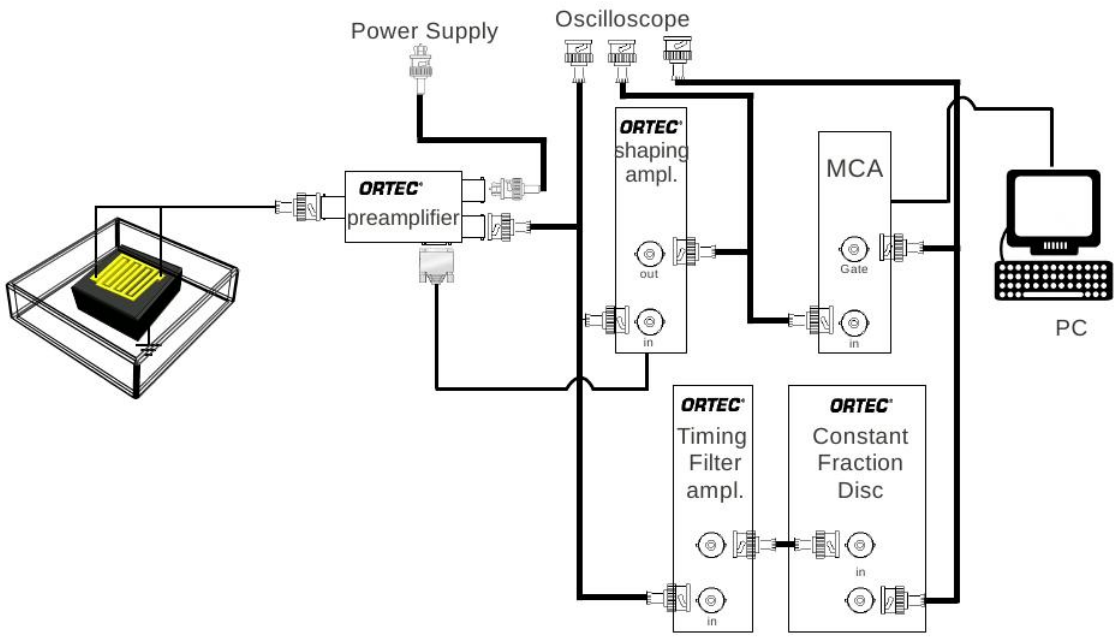

Figure 7.6: TOF system:Preamplifier ORTEC 142 IH, Amplifier ORTEC 570, MCA Multiport II (Canberra),Constant Fraction Disc ORTEC 473A and a time filter amplifiers ORTEC 474.

rising time as the time-interval between the 10% to 90% of the total amplitude of the signal. The total amplitude was the average of 10 samples after the largest point. The point at 10% was where the shape crosses the 10% of the amplitude for the last time, and the previous 5 points are smaller than 10% amplitude. For the 90% point was the same except that the followed 5 points were bigger than 90% amplitude. In this way it was possible to discriminate erroneous spike in the signal. Final the histogram of these 4000 recorded time was finally fitted by a Gaussian (the fitting was justified by the large number of recorded events). The peak position of every Gaussian represented the average rising time for this fixed voltage. Therefore every points in the figure 7.7 represents the centroid of these Gaussian. In figure are shown only the results of electrons because the results for the holes are not as clear.

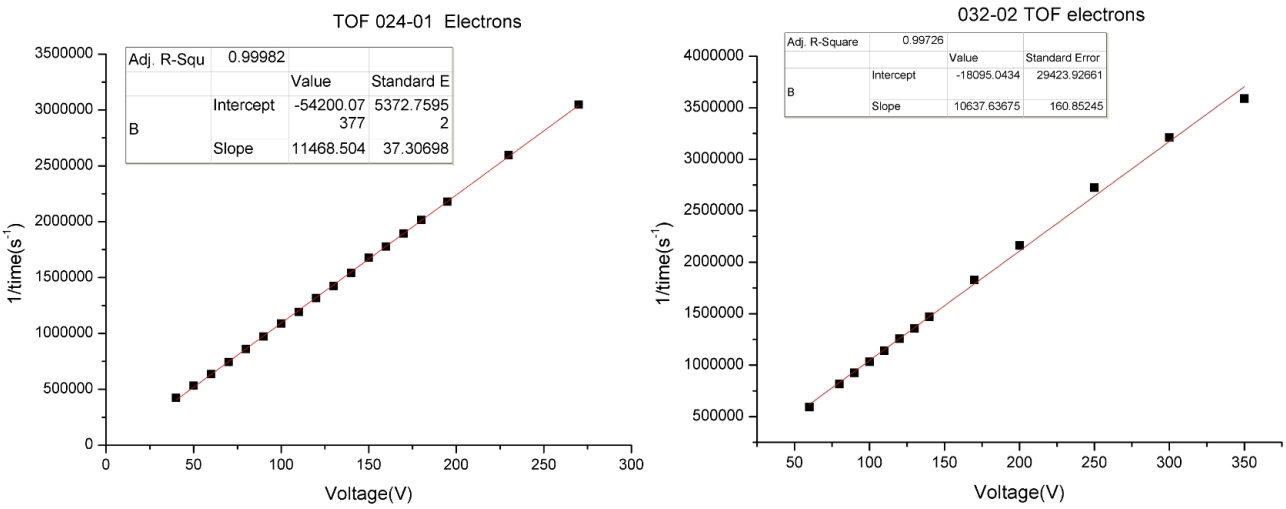

Figure 7.7: Linear fit for the TOF measures and fitting parameters for each detector

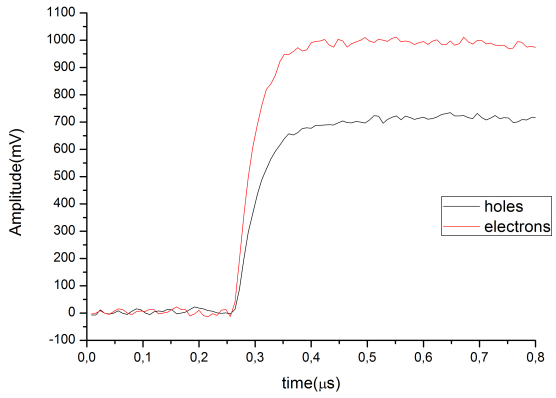

Figure 7.8: Electron and hole pulse for a bias of 230 V in 032-02 detector

In figure 7.8 it is shown a typical signal for holes compared to the electron signal at the same voltage. It is important to note that in this case the rising time of holes is compared to electrons. This is little strange because normally the mobility of holes is at most one order of magnitude less than μ_e. This strange behavior can be justified assuming that, due to high trapping process, the holes travel only a small length inside the detector before the trapping. If consider the electric field constant inside the detector the velocity is the same as the normal case but on average the distance is less, consequently the drifting time is very

short. In fact with the value of $\mu\tau$ product for holes it is possible to estimate the drift length λ_h that for $E \simeq 10^3$ and $\mu\tau \simeq 10^{-4}$ becomes $\simeq 10^{-1}\, cm = 1\, mm$. Therefore using the Hetch equation it is possible to estimate that only $e^{-1} \simeq 0.37$ holes can be collected (37% CCE) which reflect the measure of CCE. But also this explanation is not sufficient to extrapolate a relative reliable value for μ_h in the two detectors.

7.5 Spectroscopic Performance

The results of previous chapters shown that the crystal have good properties. The bulk resistance is high and comparable with commercial value, in particular both samples shown a good surface resistance after passivation process. Also the electronic properties as μ_e , τ_e and $\mu_e\tau_e$ are comparable with typical commercial value (fig 3.1). Only the hole exhibits low transport properties but in the case of a single charge sensing this does not represent a problem. In the follow table are shown all the properties of the crystals measured. In all

sample	$R_{bulk}(\Omega)$	$R_{surface}(\Omega)$	$\mu_e\tau_e(cm^2V^{-1})$	$\mu_h\tau_h(cm^2V^{-1})$	$\mu_e(cm^2V^{-1}s^{-1})$	$\tau_e(\mu s)$
024-01	$4.3 \cdot 10^{10}$	$3.6 \cdot 10^{11}$	$2.43 \cdot 10^{-3}$	$3.05 \cdot 10^{-4}$	998 ± 3	2.43 ± 0.01
032-02	$3.5 \cdot 10^{10}$	$2.8 \cdot 10^{10}$	$2.4 \cdot 10^{-3}$	$5.4 \cdot 10^{-4}$	888 ± 3	2.70 ± 0.01

Table 7.2: Properties of the two samples

the followed measurements the chatode was grounded while the two grid were connected to a dual positive power supply.

7.5.1 Spectroscopic measure

The coplanar measure system is different than the system shown in the chapter 5. For coplanar detector is necessary collect the signal from the two grids in the same time and this is possible only with two different pre-amplifier. The system is shown in Fig 7.9 The problem of using two different preamplifier is that they have in general different gain. Therefore the signal could be amplified in a different ways. On the other side the gain control is also important because can achieve the resolution decreasing the effect of the electrons trapping. For this reason in the system, as shown in figure 7.9, there are two different Time filter amplifier (TFA), set only like a gainer controllers, connected immediately after the two pre amplifiers. Before shaping amplifier the two signals must be subtracted each other in order to create a single polarity signal. The subtraction is possible with a dual sum inverter: in which one of

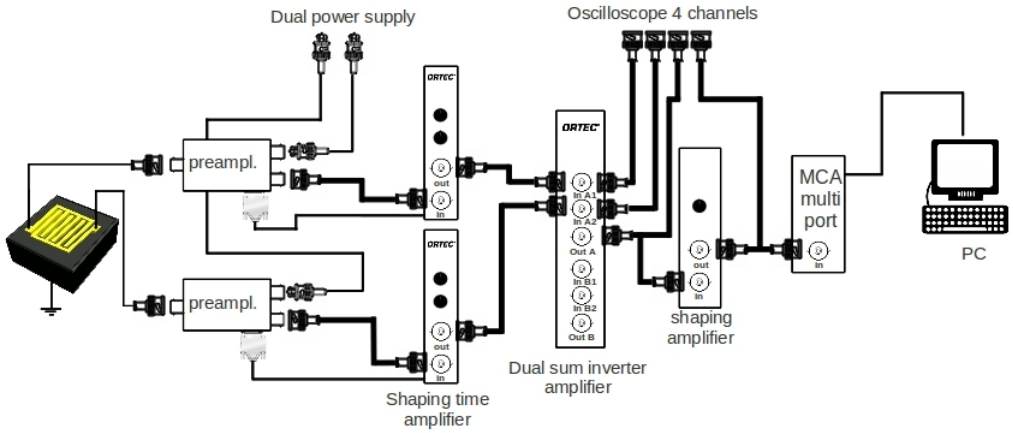

Figure 7.9: System for spectroscopic measure:2 eV pre amplifiers (A1253 and A2535), 2 time filter amplifiers ORTEC 474, Dual Sum and Inverter ORTEC 533, one Shaping Amplifier ORTEC 570 and a MCA (ToiVel)

the two signals is inverted before the sum. The inversion is done by one of the TFA: normally it is common inverting the cg signal because after the sum will be an inversion. Finally the signal out of the dual sum inverter amplifier is processed by shaping amplifier and recorded by MCA.

During the following discussion will be a distinction for two different types of operating mode one called “coplanar mode” an the other “planar mode” . The first type means the normal way of operation of a coplanar grid detector. Contrariwise the planar mode means that it is amplified only the signal of collecting grid without any correction due to the ncg: in this manner it is possible to simulate the planar device behavior. In this operating mode (planar) the ncg works as a polarized guard ring. This second operating mode is very useful for looking the real effect of the coplanar grid on the spectral resolution of the detector. In all the measurements the source was positioned on the bottom (chatode surface) as shown in fig. in the side of chatode surface for two reason: in this configuration as will show later the resolution is better. The second in this way the resolution was .

In fig. 7.10 and fig. 7.11 are shown, for the same operating condition, the comparison spectra for these two different configuration: is clear the effect of the signal correction in order to reduce the tail in the low energy side of the peak. This effect is more clear with high energy gamma ray. But, despite of the reduction in the low energy tail, the resolution is limited by an increase of noise in the high energy side that appears in the coplanar mode.

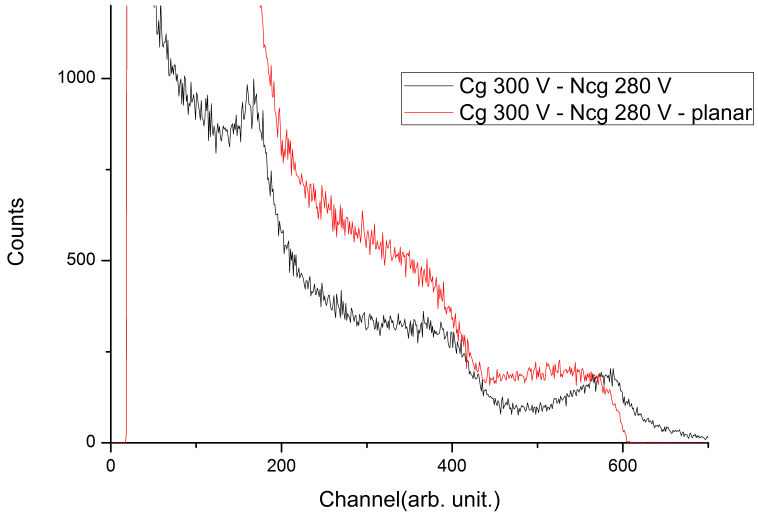

Figure 7.10: Comparison in the response of two operating mode of Detector 032-02 for ^{137}Cs peak with cg at 300V and Ncg at 280 V.

In fig. 7.12 is shown the typical signals correction of the grids and their subtraction: the images were taken by the 4 channels. oscilloscope. The picture is clear if compared with figure 5.4 with the only difference that now the linear part appears "truncated": this depending only by the interaction position. The fact was that the coplanar grid, for some reason, produced an high energy tail. The signals in fig 7.12 represent the correcting way of operating of the detector in particular the right image shown the effective correction in the signal. It is important therefore understanding what type of signal can be create in this type of detector: this will be useful for the follow discussion. In fig. 7.13 it is shown how the cg and ncg signals change with interaction depth. As shown in figure the ncg signal becomes negative when the interaction happens in proximity of the anode. It is important to note that this happens only because the hole contribution is negligible due high trapping otherwise the ncg signal could return to the baseline. Remembering that the correcting signal is the subtraction it is easy to note that in all the three cases the subtraction returns the same amplitude for each depth interaction. Therefore the energy information is the same in all the case so the resolution doesn't depend by the interaction position (this in fact is the prerogative of coplanar grid technique). But the shape of the two signals contains intrinsically the information about the interaction position. In particular when the ngc signal is only negative (there no positive

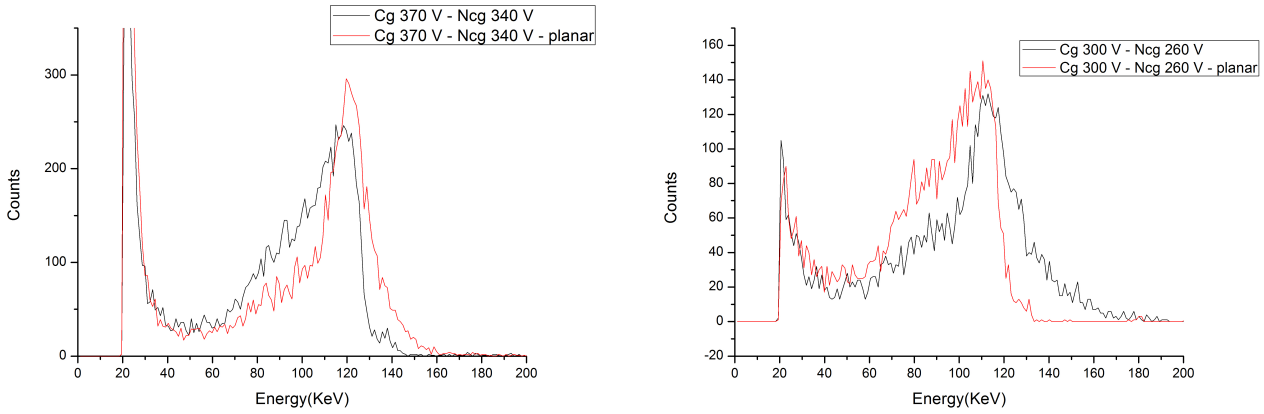

Figure 7.11: Spectra response for the two detector for ^{57}Co in particular is shown the comparison between the two operating modes: detector 032 on the left and the 024 on the right side.

parts) it means that the interaction is happened inside the Near-grid region or very close to it. The depth information is used in some detector for improving the electron trapping correction: in fact knowing the position (and the drift length) of every interactions can allow the exactly calculation of the electrons trapping. This represent an advantage respect at the gain control because it is independent to spatial non uniformity of trapping process. Hence, in addiction to single polarity sensing, the position sensing represent another important feature of the coplanar grid technique.

7.5.1.1 Correcting system for high resolution spectra.

The spectra in the planar mode of fig. 7.10 and 7.11 show the normal tail at low energy but nothing interactions with more energy than the photopeak are recorded. For this reason for example in this configuration it is possible to see the secondary emission at 136 KeV of ^{57}Co (fig. 7.11). On the other side the coplanar mode shows, as expected, the reduction of noise at low energy but ,unexpected, an increasing of the noise in the right side of the peak. The effect is to decrease the resolution of the device for example it can not resolve the same 136 KeV peak of ^{57}Co. On the other hand the coplanar mode can resolve (with very low resolution) the 662 KeV peak of ^{147}Cs, while the planar configuration does not.
In all the case this unexpected noise limited the resolution of the technique and didn't allow

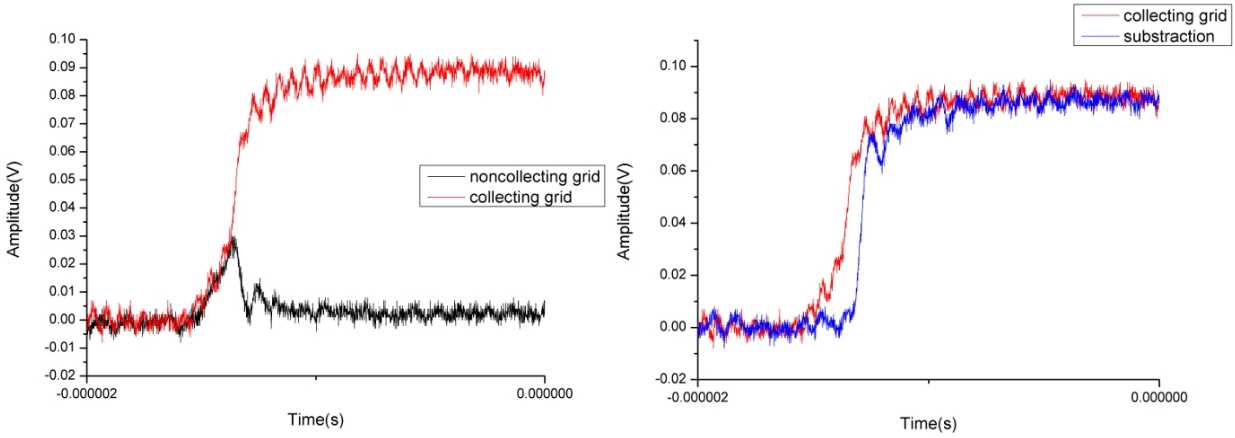

Figure 7.12: Oscilloscope signals: on the left the two signals from cg and non inverted ngc , on the right the difference in the signal before and after the subtraction of the holes contribution.

also to demonstrate unmistakably the better resolution respect the normal planar detector. In the way to correct this effect it was studied the nature of this high energy tail and two important clues were found during the experiments.

The first was found by analyzing directly the signals on oscilloscope. The signals with higher energy than the photopeak in fact were due by events with negative high amplitude ncg signal. In these cases the subtraction resulted with an expected high amplitude.

The second was found using the source ^{241}Am as "depth sensing probe". In fact the major emission of ^{241}Am is at relative low energy and ,looking fig. 4.1 , 1 mm of CZT is enough to absorb all the gamma radiation. Therefore, by positioning the source, was possible to explore 1 mm under the anode and the cathode surface and, for each one, measuring the differences between planar and coplanar mode. The result are shown in fig 7.14 . In the figure it is possible immediately observe when the high energy tail appears in coplanar mode. The results was that, with the source from the bottom (cathode surface) no important differences were shown in the two operation mode. Contrariwise with the source on the anode surface it was clear the disastrous contribution of high energy tail in the response of the detector. These two clues suggested that all the events that came from 1 mm ,at least, under the anode surface were potential "erroneous" or affected by noise.

To enhance the maximum resolution of the device a correcting system was made: the basic idea of this system was to discriminate the "erroneous" events and therefore all the signals having more energy than the major peak position. The discrimination was possible using the

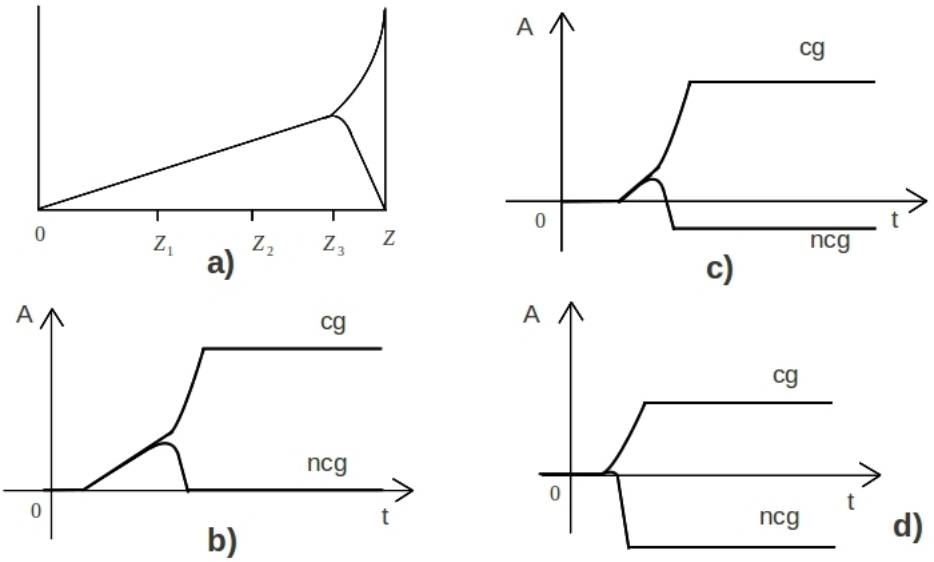

Figure 7.13: a) Induced signal as function of distance from cathode. b), c) and d) are the signals (amplitude in arbitrary unit and time) for the interactions respectively in Z_1, Z_2 and Z_3.

position information contains in the signal. As mentioned before the erroneous events came from 1 mm region under anode. The first idea was therefore to discriminate all the events with a negative ncg signal. The correcting system that was done is showed in fig. 7.15 . It is possible to see that this new system of measure is only a modification of the basic system of fig. 7.9 .The basic idea of this system was to recognize the two type of signals according to their signs. All the time that the ngc signal was negative a Constant fraction disc generated a square pulse signal. At second, the MCA were set in Non-Coincidence mode with the output of the Constant fraction disc as a Gate. In this way MCA didn't record the events when in the trigger input there was a positive square signal.
In addiction there were other two components: an amplifier and a gate delay generator. The fist was for increase the amplitude of the non collecting signal that otherwise would be smaller than the minimum of amplitude detectable by the constant fraction disc. Contrariwise the delay generator allowed to increase the time of the pulse, it was necessary because the MCA discrimination happened only if the signal was during the temporal length of the pulse. In the fig. is showed the difference between coplanar without correction, planar and coplanar with correction. As expected this discrimination process can increase the energy resolution of

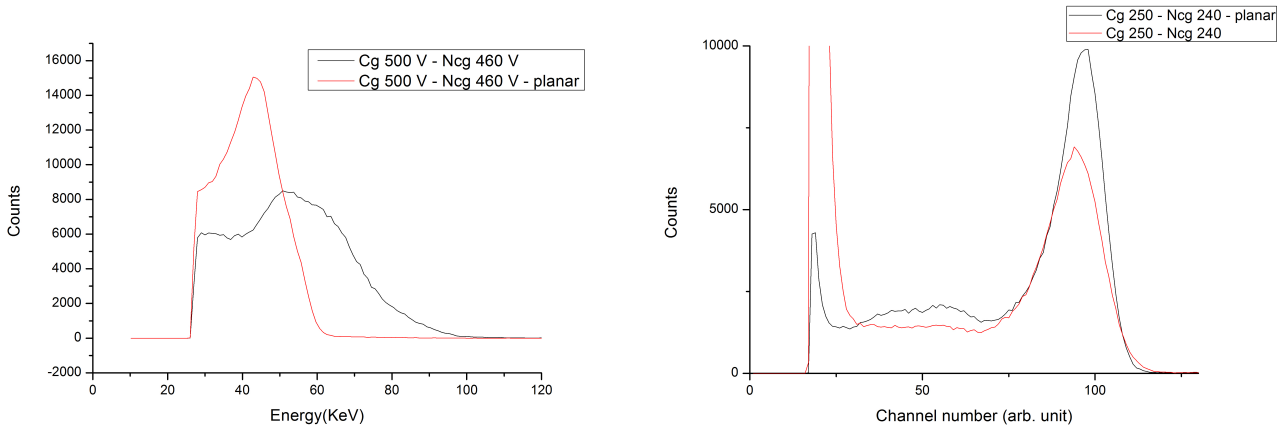

Figure 7.14: Comparison between planar and coplanar mode for the same source ^{241}Am for two different positions: left with the source from the Anode contact, on the right the response with the source near the chatode surface.

the coplanar grid. However ,on the other side, this discrimination decrease the total number of events collected by the system with decreasing in the total area of the peak. But the increasing of the energy resolution justifies the use of this system despite the decrease of the total count numbers. For this reason in all of the measure was used this system.

7.5.1.2 ^{241}Am S068.PH

The best measure were done with the source on the side of the cathode because as mentioned before the good events were created near the cathode surface. In fig. 7.16 are shown the responses of the detectors for S068.PH source. For this low energy gamma ray the coplanar grid in this work not shows a good improvement in the resolution. In this case in fact the signal amplitude in the grids was small and therefore the electronic noise contribution in the ncg in particular was counterproductive. In this case the ncg signal was only an addiction source of noise and therefore the resolution in the planar mode is better than coplanar grid mode.

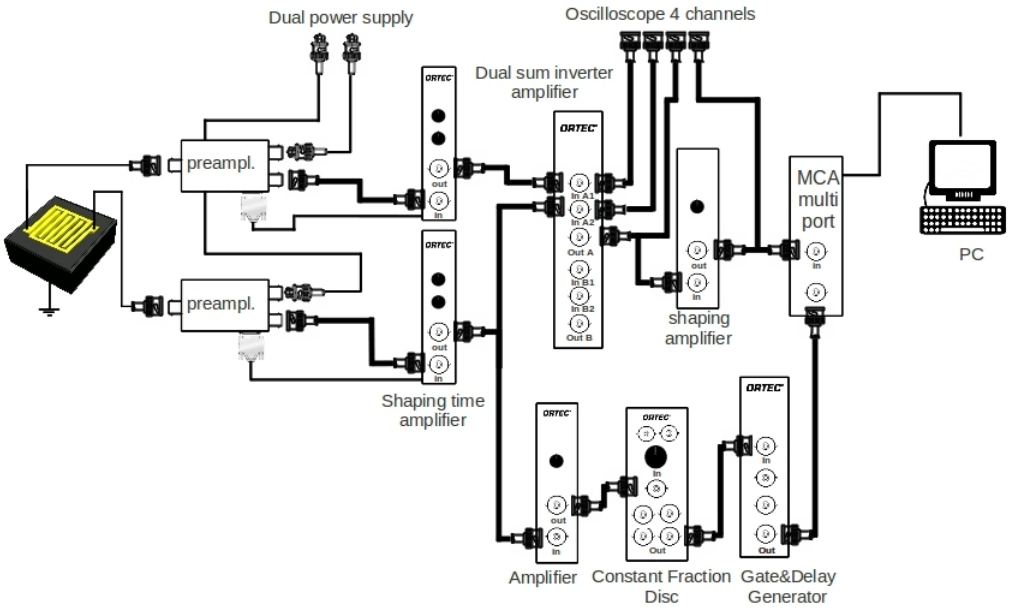

Figure 7.15: Correcting system it is similar to the system shown in fig. 7.5 there are three different components: Amplifier ORTEC 673, Constant Fraction Disc ORTEC 473A and a Gate&Delay Generator ORTEC 416 A

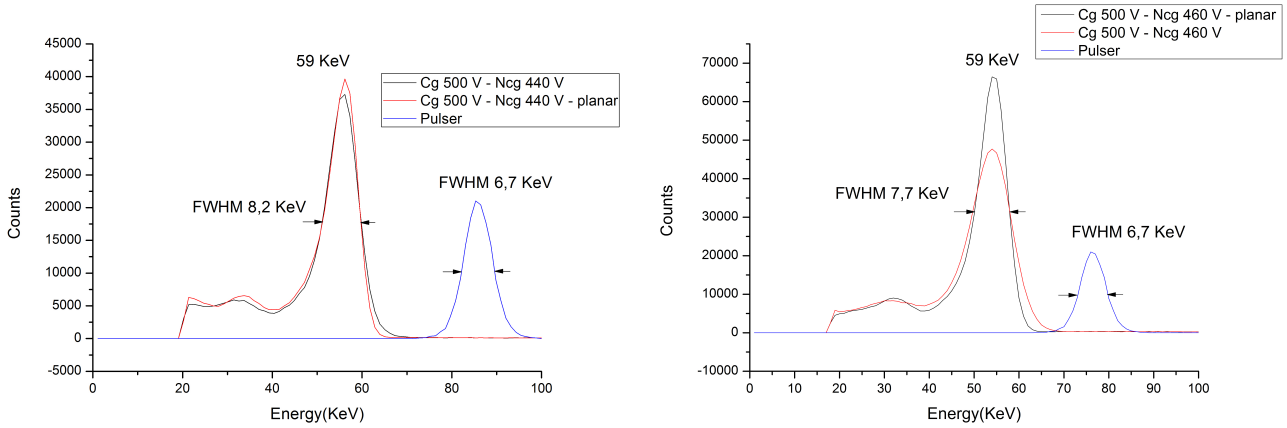

Figure 7.16: The best resolution with ^{241}Am source: on the left the response of 024-01, on the right 032-02

Using the formula 3.1 it is possible to calculate the real resolution of the detector by

substracting the contribution due to the electronic noise of the system as:

$$FWHM_{024-01} = \sqrt{(8,2)^2 - (6,7)^2} = 4,73 \tag{7.9}$$

$$FWHM_{024-01} = \sqrt{(7,7)^2 - (6,7)^2} = 3,79 \tag{7.10}$$

The resolution is 8% for 024-01 and 6,4% for 032-02.

7.5.1.3 ^{57}Co S306.PH

The gamma ray energy in this case was enough to generate in the two grid a signal significantly higher than the noise background. In the fig. 7.17 are shown the spectra responses of two detectors. It is clear that in this case the coplanar grid technique provide a real improvement in the detector performance. also in this case the source was mounted under the cathode surface.

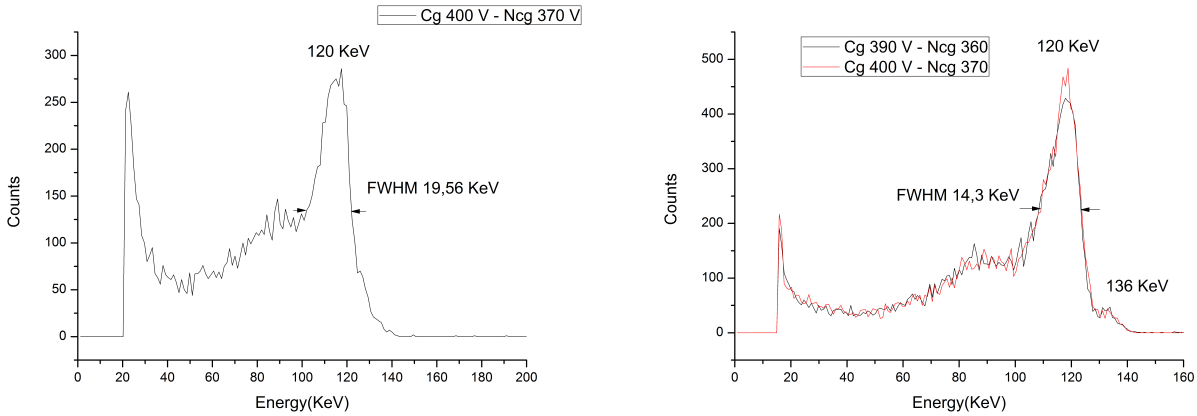

Figure 7.17: left 024 right 032

The resolution is 15% for 024-01 and 10% for 032-02.

7.5.1.4 Gain Correction

As menthioned in chapter 5 it is possible to correct the effetc due to electron trapping by playng with the gain of one grid. In fact with reducing the Ncg or increasing the Cg gain it is possible to compensate the effect due to electron trapping. In fig. 7.18 are shown the responses of 032-02 detector with different gain of Cg in order 1, 1,1 and 1,2 respect the Ncg

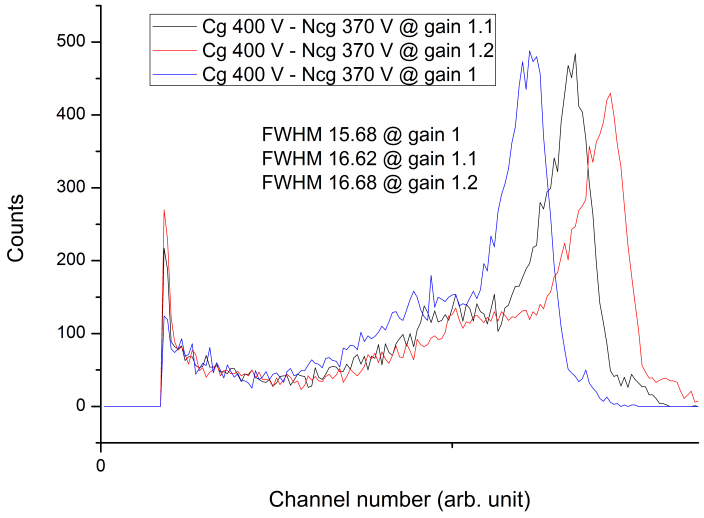

Figure 7.18: 032-02 response detector at ^{57}Co source.

that was assumed at gain 1. As shown in the picture this system was not enought sensible to allow the compensation of electron trapping. The effect of the gain was only to enanche the noise in the Cg channel and therefore dereasing the resolution of the detector.

7.5.1.5 ^{137}Cs S227.PH

This represent the common source for showing the effective work of coplanar grid device. In fig. 7.19 are shown the spectra of two detectors and the comparison with the relative planar mode.

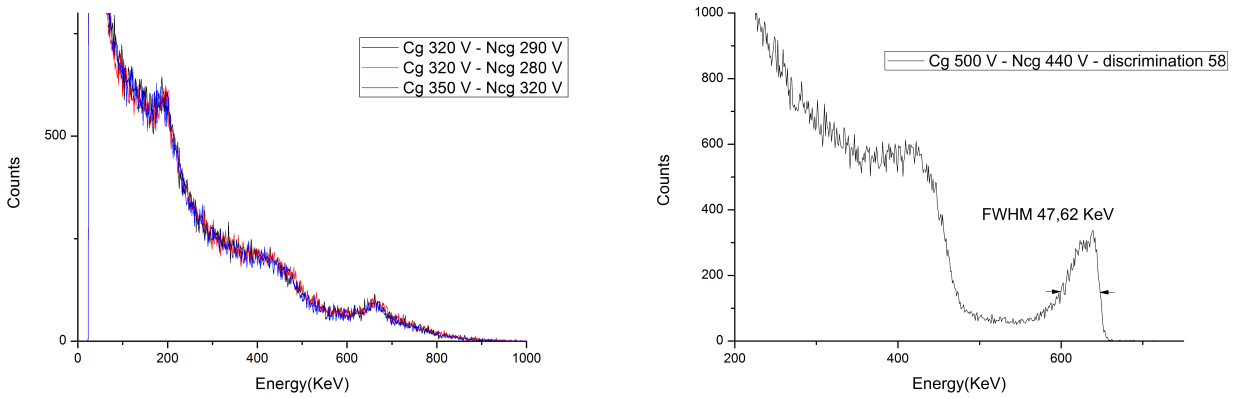

Figure 7.19: left 024 right 032

In particular with 032 detector was found the best resolution of 7% shown in fig. 7.20

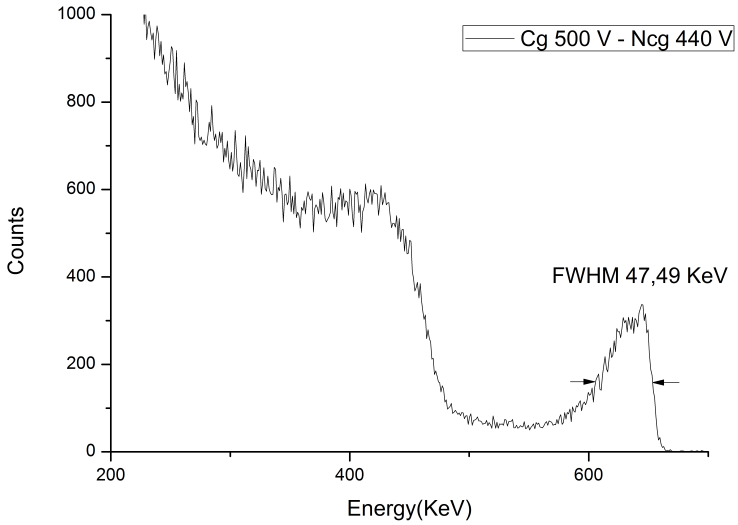

Figure 7.20: The best resolution in the 662 KeV peak of ^{137}Cs in 032-02 detector

with the same detector other measure were done in the way to analyze the number of discriminate events due to the correcting system as function of grids voltage.

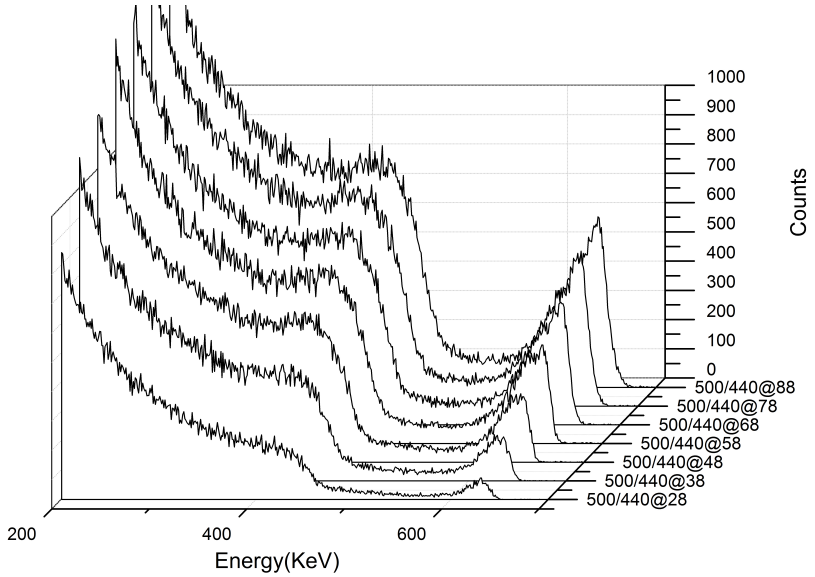

Figure 7.21: Discrimination effect in detector 032-02 for 662 KeV peak of ^{137}Cs.

The result confirm the lost in count number due by the discrimination.
The effects of the correcting system in the 032-02 detector were investigated comparing the FWHM and Area of the peal changing the voltage between grids. In table 7.3 are shown these results.

Voltage	Non Correcting System		Correcting System		%of good events
Cg(V)/Ncg(V)	FWHM	$Area_{NCS}$	FWHM	$Area_{CS}$	$(Area_{CS}/Area_{NCS}) \cdot 100$
500/500	88	19160	59.9	8175	43%
500/490	88.1	21749	56.9	8537	39%
500/480	85.5	28036	54.5	9761	35%
500/470	82.2	31970	49.6	10709	33%
500/460	73.9	37714	41.8	11770	31%
500/450	64.4	40586	47.3	11983	30%
500/440	60.5	40796	39.7	12518	31%
500/430	60.5	42348	43.2	12620	30%
500/420	73.6	41670	47	12365	30%
500/410	80.1	38388	51.2	12424	32%

Table 7.3: Effects of correcting system, for a fixed discrimination level in 032-02 detector. The measures of FWHM and Area were done by MCA Software in the 662 KeV peak of ^{137}Cs.

The table explains well the effect of the correcting system in order to increase the resolution. But also the effect is to reduce the counts in the peak, in particular only an average of 30% are not discriminate that means that, probably, only the vents that happen a 1 mm under the Cathode surface are good. In 3 mm detector this effect is also stronger due to the relative low thickness of the device, maybe with more thickness the effect of the tail can be reduce.

7.5.2 Nature of the high energy tail

One of the first hypothesis was the sharing charge between grids The first is that the sharing charge can only decrease the real signal and therefore increasing the low energy tail. On the other hand if the high energy tail was due by the sharing this effect could be changed by the difference voltage between the grids. In fig 7.22 is shown the change in the ^{137}Cs peak changing the voltage of the cg and ncg. It is clear that the sharing charge is not negligible but the high energy tail not depend by this phenomenon. Also the dimension of the near-grid region does not explain this strong reduction in the resolution in particular because this region must be as larger as the strip pitches ($\approx 250\mu m$). Moreover the strips pitch are comparable to other device in literature.

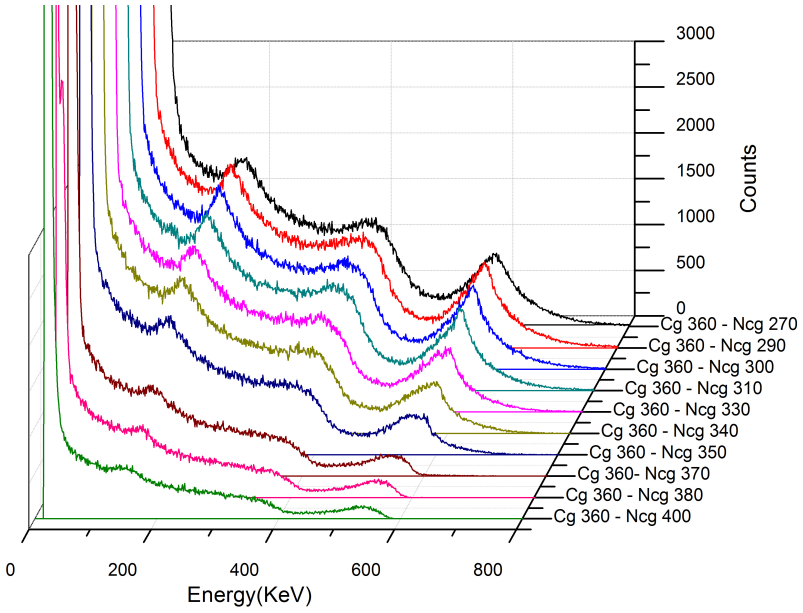

Figure 7.22: 662 KeV ^{137}Cs peak shape for different cg/ncg voltage

Looking the spectra in the original work of Luke, the peak of ^{137}Cs shown the same tail at high energy (fig 7.23 b)) although less than in this work. Probably because the spectra was measured with a 5 mm thickness and therefore the effect is less than a 3 mm thickness. Zong He et al. found that the problem was due by the geometry of the grids. In particular they found that the erroneous events happened near the anode surface because, in this region, the weighting potential shown non-uniformity behavior. The geometry of fig. 6.1 is called I generation and exhibited a spatial non uniformity in the weighting potential along the surface of the anode. Looking fig 6.1 it is possible to see that the boundary conditions are different for the external strips compared with the central. For example the external cg strip has only one adjacent ncg strip, contrariwise one central strip has two adjacent strips. The strips have all the same dimension and therefore the induced charge in the Ncg is different in these two cases.

The calculation done by He at al. shown that the non uniformity is maximum in the region of 1 mm under the anode which is in agreement with the previous conclusions. This is clear looking the right part of figure 7.23 . The solution of this problem is therefore a new geometry of the contact in stead to increase the uniformity in the weighting potential. Also an external electrodes (as a guard ring) can increase the spatial uniformity of the wp.

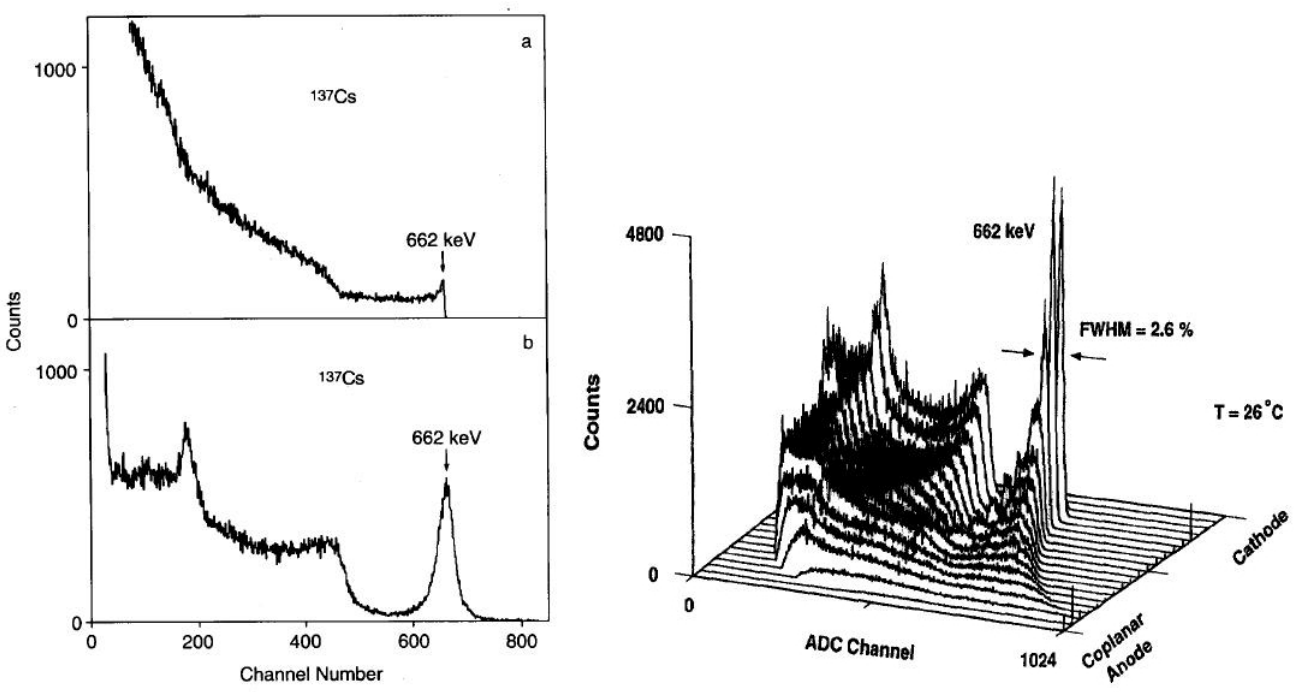

Figure 7.23: Figure on the left the 662 peak of ^{137}Cs in the original work of Luke in particulate a)planar detector and b) coplanar detector. Note the high energy tail in the right side of 662 peak in figure b). The right figure shows the detector response for different interaction depth [] measuring with a I generation coplanar grid geometry.

7.5.3 List of the sources

In table 7.4 there is list of the sources were used in this work:

Source	Name	Activity (KBq)[1]	α(MeV)	γ(KeV)(probabilities)[2]	
^{241}Am	S037.RG	185	4.952265*	59	
^{241}Am	S068.PH	351.8	/	59	
^{57}Co	S306.PH	2.7	/	122(85%),136(11%),14(9%)	
^{147}Cs	S227.PH	258.2	/	662(85%)	

Table 7.4: Sources used in the work. [1]The activity was calculate in date 2/09/10. *The energy was measured in Radiation Laboratory University of Surrey with a Si photodiode, the energy is lower than predicted (5.48574 MeV[Knoll]) due to self absorption effects. The values[2] are taken by [Knoll]

Chapter VIII

Conclusion

The effective improvement due coplanar grid technique was proved in particular for high energy gamma ray (^{57}Co and ^{137}Cs) also for small thickness detector. In particular the 662 KeV peak of ^{137}Cs was seen for the first time in the IMEM group samples. The transport measure proved the good quality of the $Cd_{0.9}Zn_{0.1}Te$ grown with full encapsulate vertical Bridgman and in particular the electronic properties are comparable to commercial crystal. Also the $\mu_h\tau_h$ was measured for the first time in the IMEM samples.
Not very good resolution was found for both detectors due non uniformity effects in the weighting potential. As shown these effect are due by the contact geometry that, unfortunately was fixed by the mask. To increase the resolution was done a correcting system and a resolution of 3.7% was found in the ^{137}Cs peak with the 032-01 detector. This detector in fact despite the higher leakage current showed better resolution than the 024-01.
It was also difficult to compare the resolution of 3 mm thickness detectors made with literature because the standard thickness of coplanar grid detectors are in the range between 0.5 and 1 cm.
Finally some ideas for future developing of CZT Coplanar Grid detectors in the way to enhance the resolution:

- Increase the thickness of the samples (5 mm as starting point)

- Increase the uniformity of the weighting potential by adding a guard ring around the coplanar grid contacts of fig. 6.1.

- Design a new contact geometry (3th generation). In fig. 8.1 there is a new contact geometry designed myself considering the works done by Zong He et al. and Amman and Luke. The total area of the contact is $6x6\ mm^2$, the number of strips is the same as in the geometry of fig. 6.1 but now the dimension of the strips and the pitch are reduced. This because the good insulating properties of the surface allow reducing the

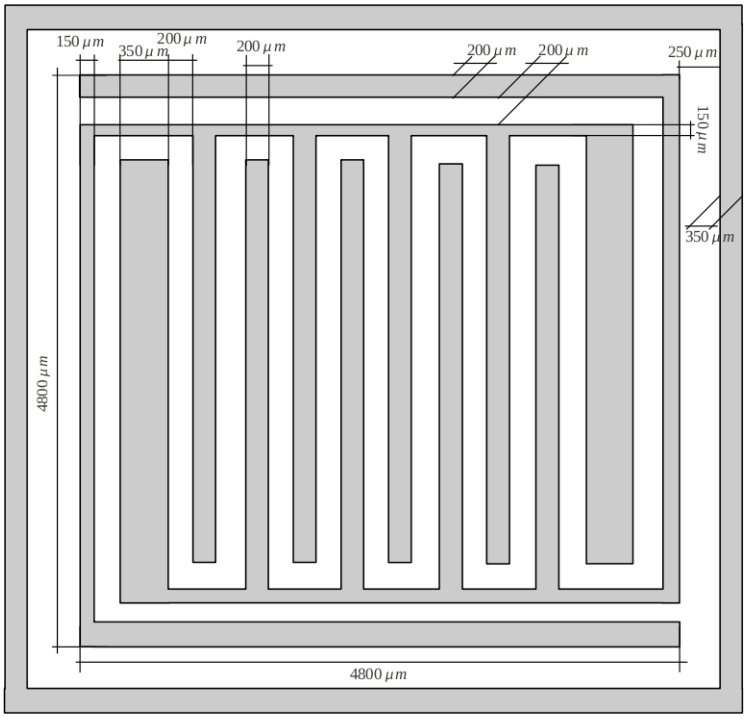

Figure 8.1: 3th generation coplanar grid geometry designed myself following the references [][][].

dimension of the strips and pitches, decreasing therefore the non linear region under the grid. There are no problems for bounding because how shown in fig. 6.1 left the dimension of bubble of glue are always less than 350 μm. Following the reference in this new geometry there is a guard ring and the external strips are bigger than the other. It is possible in this way reduce the effects due to spatial non uniformity of weighting potential. Also the total dimensions are comparable to the previous geometry and therefore it is possible to compare the two geometry and the detector response.

Appendix A

In this work was used a negative photoresist ma-N 415, is composed of novolak and azide sensitizers. This resist is sensitive to light in the middle UV in a range between 300-380 nm and it allows a resolution up to 0.1 μm [20].

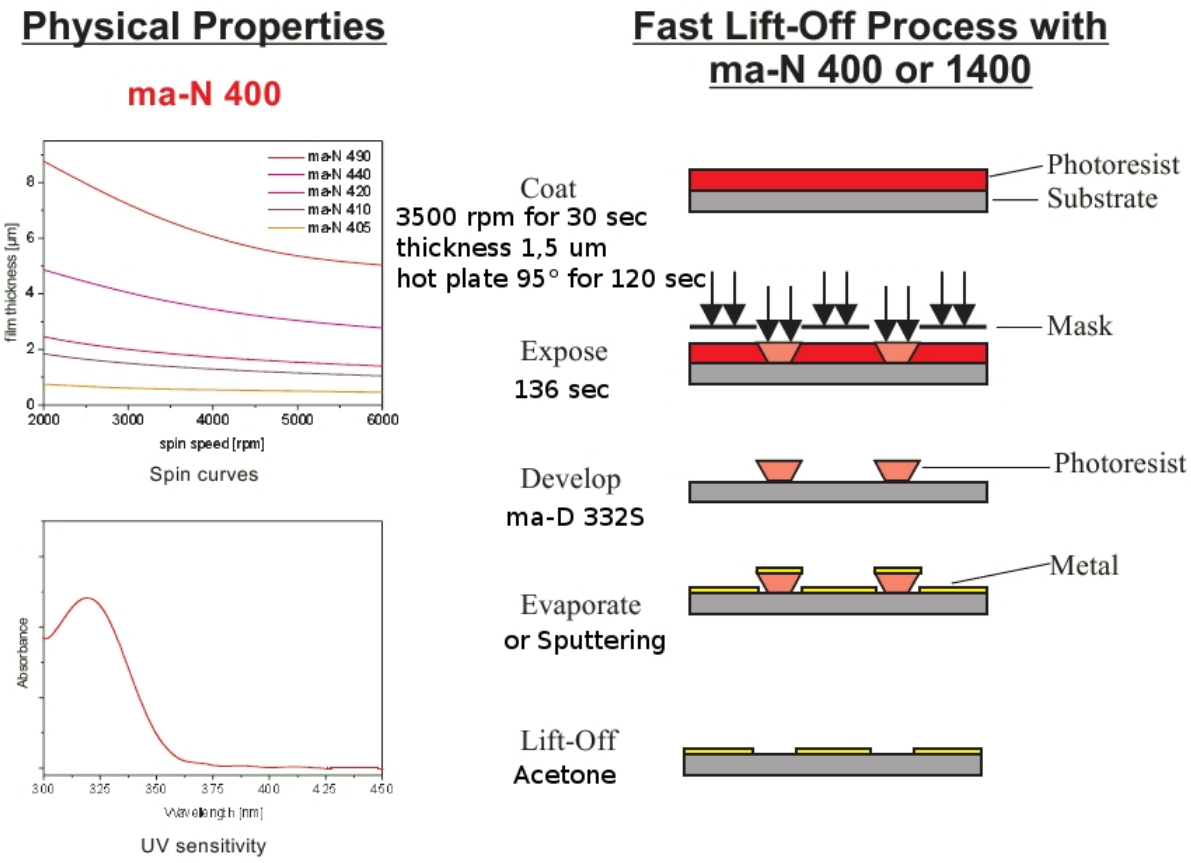

Figure 8.2: Lift-Off process for ma-N 415 photoresist

Appendix B

Equipment

Glue for Wire Bonding

Code Agar Scientific N° G3349

Description: This is a two part electrically conductive silver epoxy suitable for mountingSEM samples, and for other applications such as repairing circuit boards for solderless electronic connections.

Volume Resistivity: $< 0.001\ \Omega \cdot cm$

Adhesion: Excellent

Silver Paint

Code: Agar Scientific N°G3648

Description: This is the genuine replacement for DAG 915 which is used widely not only in electron microscopy but in electronic circuitry for capacitor terminations, electrostatic screening, coating of UHF reflectors and electroplating on non conductors.

Unipol 810

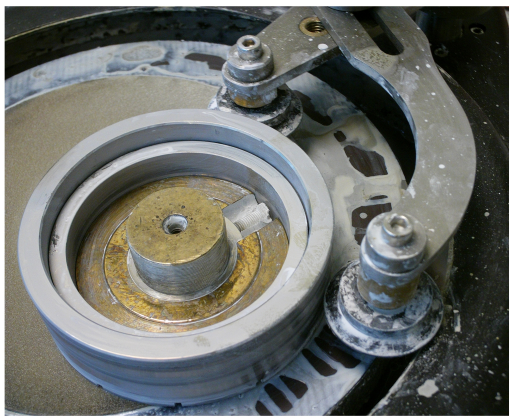

Figure 8.3: Lapping machine UNIPOL 810, on the right a detail of the sample holder.

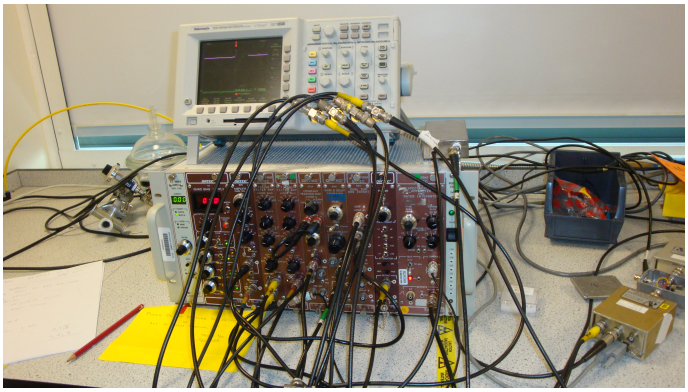
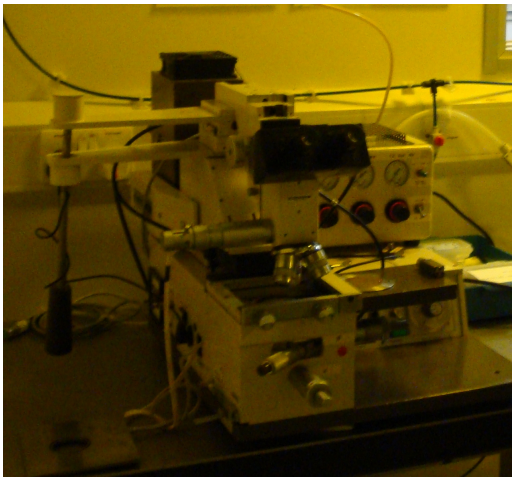

Figure 8.4: Left : image of the correcting system used in spectroscopic measurements. Right: Karl Suss MJB-3 Mask Aligner.

Sputtering EMITECH K575X

Figure 8.5: EMITECH K575X

Vacuum: 0.1 to 0.05 torr

Sputtering Voltage: 100 to 150 Voltage

Current: 0 to 50mA

Deposition: 0 to 50nm/min

Grain size: less than 5 nm

Temperature rise: less than 10°

Features: allows the deposition of noble and oxidizable materials

References

[1] H. Spieler: Semiconductor Detector Systems, Oxford University Press, 2005

[2] [M. E. Ozsan, P. J. Sellin, P. Veeramani, S. J. Hinder, M. L. T. Monner, G. Prekas, A. Lohstroh, M. A. Baker. (2010) Chemical etching and surface oxidation studies of cadmium zinc telluride radiation detectors. InterScience]

[3] GF Knoll, Radiation Detection and Measurement, 3rd ed. (Wiley, New York, 2000).

[4]

[5]

[6]

[7]

[8]

[9]

[10]

[11]

[12]

[13]

[14]

[15]

[16]

[17]

[18]

[19]

[20] A. Voigt, G. Gruetzner, E. Sauer, S. Helm, T. Harder, S. Fehlberg, J. Bendig „A series of AZ-compatible negative photoresists“ Proc. SPIE 2348 (1995), 413–420

[21]

[22]

[23]

[24]

[25]

[26]

[27]

[28]

[29]

[30]

[31]

[32]

[33]

[34]

[35]

[36]

[37]

[38]

[39]

[40]

[41]

[42]

[43]

[44]

[45]

[46]

[47]

[48]

[49]

[50]